Progress in Oceanography 104 (2012) 80–98

Contents lists available at SciVerse ScienceDirect

Progress in Oceanography

journal homepage: www.elsevier.com/locate/pocean

Seasonal variability on the West Florida Shelf

Yonggang Liu *, Robert H. Weisberg

College of Marine Science, University of South Florida, 140 7th Ave. South, St. Petersburg, FL 33701, USA

ARTICLE INFO

Article history:
Received 11 January 2012
Received in revised form 12 June 2012
Accepted 15 June 2012
Available online 28 June 2012

ABSTRACT

The seasonal variations of the West Florida Continental Shelf (WFS) circulation and sea level are described using observations of velocity from an array of moored acoustic Doppler current profilers and various ancillary data. With record lengths ranging from 3 years to over a decade, a robust seasonal cycle in velocity is found, which varies across the shelf in a dynamically sensible way. Over most of the inner shelf these seasonal variations are primarily in response to local forcing, through Ekman-geostrophic spin-up, as previously found for the synoptic scale variability. Thus the inner shelf circulation is predominantly upwelling favorable from fall to spring months (October–April) and downwelling favorable during summer months (June–September). Seaward from about the 50 m isobath, where baroclinicity becomes of increasing importance, the seasonal variations are less pronounced. Over the outer shelf and near the southwestern end of the WFS, the seasonal variations are obscured by the deep ocean influences of the Gulf of Mexico Loop Current and its eddies.

The seasonal variations in sea level are also robust. But unlike the velocity, these extend across the entire WFS and into the deep Gulf of Mexico. These seasonal sea level variations arise from two influences, one static, the other dynamic. The static influence projects onto the WFS by the static seasonal rise and fall of the Gulf of Mexico sea level due to heating and cooling (also occurring on the shelf). On climatological average, this ranges by about 0.12 m, with a minimum in February and a maximum in August and deriving primarily from the density variations over the upper 100 m of the water column. Such climatologically averaged variation due to temperature and salinity is also seen in satellite altimetry. An additional dynamic influence of about 0.06 m occurs over the inner shelf by the Ekman-geostrophic spin up to the seasonally varying winds. Together, the static and dynamic ocean responses result in a climatologically averaged coastal sea level variation at the central (vicinity of Tampa Bay to Charlotte Harbor) region of the WFS of about 0.18 m after adjustment for the inverted barometer effect, which adds about another 0.06 m for a total climatologically averaged annual sea level range of about 0.24 m.

1. Introduction

By connecting the coast with the deep ocean, the continental shelf circulation determines the coastal ocean transport of material properties of either land or deep ocean origin. These connections, in turn, provide the underpinnings for continental shelf ecology. Consider, for instance, the influence of the circulation on harmful algae (e.g., Weisberg, 2011), or the fate of hazardous materials, as highlighted for the *Deepwater Horizon* oil spill by Liu et al. (2011a and the chapters therein). Descriptions and understandings of the continental shelf circulation are therefore of fundamental important for all coastal ocean processes.

Here we consider the seasonal circulation of the West Florida Continental Shelf (WFS), an eastern Gulf of Mexico shelf that is wide enough to distinguish specific dynamical regimes. Following the discussions of Li and Weisberg (1999a,b), Weisberg et al. (2001) and Weisberg et al. (2009a), the WFS may be partitioned into outer, middle and inner shelf regions, plus a near shore region embedded within the inner shelf. The outer shelf extends an internal Rossby radius of deformation inward from the shelf break, providing a buffer zone between the deep ocean and shelf. The inner shelf is defined as the shallow, frictionally controlled region where surface and bottom Ekman layers interact through divergence and where, under stratified conditions, these Ekman layers may be separated from one another. The near shore region is where estuarine-imposed salinity gradients may add an additional baroclinic effect to the inner shelf. If the shelf is wide enough to separate the inner from the outer shelf, the middle shelf comprises the region in between. These distinctions are manifest for the WFS both in observations and numerical circulation model simulations, and they allow us to abandon arbitrary geographical definitions. For the central portion of the WFS (vicinity of Tampa Bay to Charlotte Harbor) where most of our attention is focused, the outer shelf extends roughly 30 km in from the shelf break (located approximately at the 80 m isobath) and the inner shelf extends out to about the 50 m isobath.

* Corresponding author.
E-mail address: yliu@marine.usf.edu (Y. Liu).

0079-6611/$ - see front matter © 2012 Elsevier Ltd. All rights reserved.
http://dx.doi.org/10.1016/j.pocean.2012.06.001

Our observations of the WFS circulation began in 1993. These were systematically expanded in 1998. Weisberg et al. (2009b) discuss the long-term mean circulation and inferences on how it is forced by winds, heat fluxes, and interactions with the bounding deep ocean. As an extension to that work we now consider the seasonal variations of the WFS circulation (and sea level) about the long-term means. With emphasis primarily on the inner shelf, we now have records (some continuous for over a decade) of sufficient length to establish (within standard error definitions) both a mean velocity field and a climatological seasonal cycle. Being that the WFS is largely forced by local winds and heat fluxes over the shelf and that these local forcing functions exhibit well-defined seasonal variations, it follows that robust seasonal cycles should also exist in the circulation and sea level. Such was inferred by Yang and Weisberg (1999) and then described by Weisberg et al. (2005) and Liu and Weisberg (2007) using a more limited in situ data set. Carlson and Clarke (2009) then inferred a seasonally varying along-shelf geostrophic flow from satellite altimetry over the northern WFS.

As with all continental shelf regions, our studies began with the premise that the WFS circulation varies over a broad range of time and space scales (e.g., Boicourt et al., 1998). Direct measurements of the WFS circulation using in situ, moored current meters started in the 1970s (e.g., Niiler, 1976; Price et al., 1978; Weatherly and Martin, 1978; Blaha and Sturges, 1981; Mitchum and Sturges, 1982; Marmorino, 1983a,b; Halper and Schroeder, 1990; Weatherly and Thistle, 1997), but these were mostly of short duration, rendering inferences on the seasonal variations not possible. Such inferences initially derived from purposeful deployments of drift bottles that subsequently washed up on beaches (e.g., Tolbert and Salsman, 1964). The use of satellite tracked drifting buoys (Ohlmann and Niiler, 2005; DiMarco et al., 2005) added to these inferences, but fell short of distinguishing a seasonal cycle due to the Lagrangian nature of drifters, that require many more repeated deployments to avoid biasing by either initial conditions or spatial avoidances. For instance, a "forbidden zone" for the southeastern portion of the WFS was described by Yang et al. (1999) as a region of avoidance by surface drifters deployed farther north due to the upwelling nature of the circulation. With surface drifters tending to avoid the inner shelf because of a general upwelling favorable circulation, it is understandable that drifters alone would have difficulty in defining a seasonal cycle, especially over the inner shelf.

Longer-term in situ measurements with moored acoustic Doppler current profilers (ADCPs) began in 1993, first at a single, geographical mid shelf location (Weisberg et al., 1996) and then at multiple locations across the shelf (e.g., Weisberg et al., 2000, 2001, 2005, 2009b; Meyers et al., 2001; Liu and Weisberg, 2005a). With systematic observations acquired shoreward from the 50 m isobath from 1998 to 2001, a seasonal cycle, with the inner shelf currents tending to be upwelling from October to April and downwelling from June to September, began to emerge (Liu and Weisberg, 2005b, 2007; Weisberg et al., 2005). Moreover, these seasonal variations appeared to derive from the combined forcing by local winds and heat fluxes, as inferred from numerical circulation model simulations (e.g., Yang and Weisberg, 1999; He and Weisberg, 2002, 2003). Yet, 3 years of data at that time were not sufficient to counter the lack of a seasonal cycle inferred by Ohlmann and Niiler (2005) and DiMarco et al. (2005) through analyses of satellite tracked surface drifters. Establishing a robust seasonal cycle for the WFS circulation had to await longer record lengths.

Unlike the currents, coastal sea level data exist over a much longer interval. WFS coastal sea level responses to synoptic scale weather forcing (winds and surface pressure) were discussed by Marmorino (1982, 1983a,b), Mitchum and Sturges (1982), and Cragg et al. (1983). An analytical, wind-forced continental shelf wave model was the used by Mitchum and Clarke (1986a,b) to explain the synoptic scale coastal sea level variations in response to the along-shelf component of wind stress, making accommodation for inner shelf frictional boundary layer effects through parameterization. But despite the strong statistical inference on sea level response to along-shelf wind stress we also know that the across-shelf component of wind stress plays a role in the sea level set up over the inner shelf (e.g., Li and Weisberg, 1999a,b; Tilburg, 2003; Liu and Weisberg, 2005a, 2007; Fewings et al., 2008). For the WFS, in particular, and using a combination of observations from moored ADCPs, shipboard hydrography, bottom pressure gauges, coastal tide gauges and meteorological stations collected from September 1998 to December 2001, Liu and Weisberg (2007) diagnosed the various dynamical contributions made to the sea level variations shoreward from the 50 m isobath. For coastal sea level variations at time scales corresponding to the synoptic scale weather, it was found that the across-shelf sea surface slopes attributed to the vertically integrated along-shelf currents, the baroclinic additions to these, and the direct set up by the across-shelf component of wind stress all contributed to the sea level variations at the coast with similar magnitudes. At longer time scales, roughly half of the sea level variations estimated at the 50 m isobath were attributed to steric height changes occurring there. Based on these previous results it seemed instructive to consider the sea level variations in their totality with respect to both local (shelf-wide) and deep ocean contributions, especially at the seasonal time scale where large static steric variations are known to exist.

To put these introductory remarks into context, Fig. 1 shows variance distribution functions (normalized, cumulatively integrated variance density spectra) calculated for sea level at St. Petersburg, FL and for the depth-averaged across-shelf and along-shelf components of velocity at two WFS moorings, one (C11) situated on the 20 m isobath and the other (C12) at the 50 m isobath. Referencing Fig. 2, the along-shelf direction (principal axis orientation of the depth-averaged sub-tidal currents) roughly aligns with the local isobaths, with positive directed approximately north–northwest, and the across-shelf direction is normal to the along shelf direction with positive directed onshore (e.g., Liu and Weisberg, 2005a; Weisberg et al., 2009a,b). The power spectral density functions are normalized to unit variance over the frequency interval from zero to the Nyquist frequency (0.5 cph). With the variances provided in the figure legend, these distribution functions apportion variance across different frequency intervals (e.g., seasonal, synoptic, tidal). Both the sea level and the along-shelf component of velocity at the 20 m isobath show a similar jump at the annual time scale. The along-shelf component of velocity at the 50 m isobath also possesses seasonal variance, but less well defined. The across-shelf components of velocity vary more subtly at low frequency. Thus a structure exists across the shelf that requires explanation with respect to the dynamics and thermodynamics involved, and despite the small amount of variance at the seasonal cycle relative to the tides and the synoptic band variances, these are still of major ecological and geological importance. Ecologically, for example, the seasonal variations in the currents influence the spatial distributions of organisms, and geologically, the fact that sea level tends to be some 24 cm lower (higher) in winter (summer) months, influences the long term sediment transport due to seasonally varying wave energy flux.

The present paper extends the long-term mean circulation work of Weisberg et al. (2009b), using the same data set, augmented by sea level and other ancillary data, to address the seasonality of the WFS circulation and to examine the contributions to the coastal sea level variations observed at the seasonal time scale by both local and deep ocean effects. Our intent is to clarify the existence and origin of the seasonal cycles in the circulation and sea level on

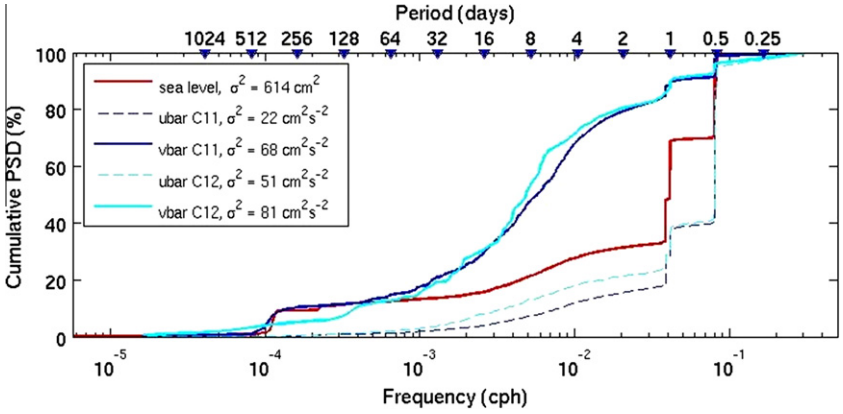

Fig. 1. Cumulative power spectral density of St. Petersburg sea level and depth-averaged across- and along-shelf velocity (ubar, vbar) at mooring C11 (20 m site) and C12 (50 m site) on the West Florida Shelf. The spectra are normalized to have unit variance over zero to Nyquist frequency band. The variances (σ^2) of the time series are shown in the legend.

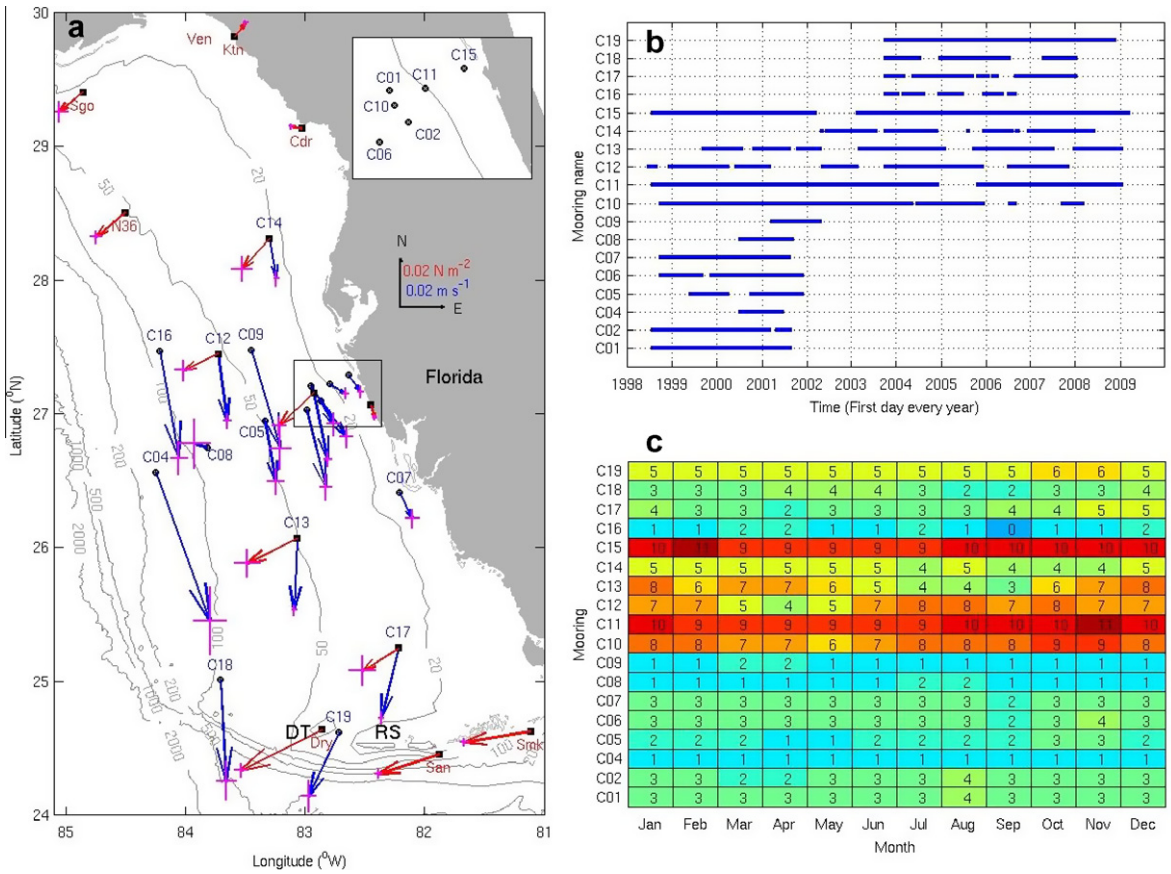

Fig. 2. Locations and timelines of long-term moorings on the West Florida Shelf. (a) Mooring locations and depth-averaged mean current (blue) and wind stress (red) vectors (adapted from Weisberg et al., 2009b). The standard errors ε of the mean values μ are shown as crosses ($\mu \pm \varepsilon$) at the arrow heads. Also shown on the maps are isobaths in meters. DT and RS designate Dry Tortugas and Rebecca Shoals, respectively. (b) Timeline of moored ADCP measurements. (c) Checkerboard showing the distribution of the moored data (number of years) among the 12 months for all the moorings. Records with lengths longer than 20 days during a month are counted as a month. (For interpretation of the references to color in this figure legend, the reader is referred to the web version of this article.)

the WFS. Observations and data processing are described in Section 2. The seasonality of the WFS currents is described in Section 3, where monthly mean climatologies are provided for winds, depth-averaged currents, and velocity profiles. The seasonality of the sea level variations and their contributing factors are then analyzed in Section 4. Findings are discussed in Section 5, and Section 6 provides a summary.

2. Data and processing

Velocity data are drawn from in situ moorings deployed on the WFS over the approximate 10 year period, 1998–2009. Within this time interval, a total of 18 sites were occupied by the University of South Florida, College of Marine Science, Ocean Circulation Group (USF-OCG), each for durations of a year or longer. As shown in

Fig. 2, these sites extended from the 10 m isobath (near shore) to the 162 m isobath (shelf slope). The measurements were all made with RD-Instruments (RDI) acoustic Doppler current profilers at nominal frequencies of 1200, 600, 300 kHz depending on water depth. Upward looking broad-band ADCPs with 20° transducer configurations and varying (depth appropriate) frequencies were mounted in trawl-resistant bottom racks and deployed on the sea floor at C11, C15 and C19. Upward looking 600 kHz, narrow-band ADCPs with 30° transducer configurations were mounted within subsurface floats and deployed near the bottom at C04, C08 and C18. All of the other sites were occupied by either narrow-band (initially) or broad-band (almost all after 2002) ADCPs mounted on surface buoys and looking downward. Transducer locations from either the surface or the bottom, blanking distances, bin sizes, and sampling schemes varied with moorings, specific instruments, and firmware revisions. The bottom racks and the surface buoys generally had the transducer heads located approximately 0.5 m from the bottom and 1.5 m from the surface, respectively, and these utilized either 0.5 m or 1.0 m bins. The ADCPs on subsurface buoys utilized 4 m bins. With a few exceptions (early in the program) all of the ADCPs used one second ping rates averaged over the first 6 min of each hour to produce hourly velocity estimates. Multiple deployments were generally made for each site, with each deployment lasting from several months to more than a year. The data from each of these deployments were interpolated onto uniform vertical levels and concatenated in time to form extended time series. Excluding gaps, the record lengths ranged from one to more than 10 years (Table 1). After editing, we found essentially no differences in velocity data that were collected using either upward or downward looking instruments (Mayer et al., 2007). Additional information on the moorings and the data editing procedures are provided by (Liu and Weisberg, 2005a,b, 2007).

Other data used herein include meteorological observations and analyses, sea level records, and hydrographic climatology. Hourly meteorological observations were recorded at some of the USF-OCG surface buoys (C10, C12, C13, C14, C17) and at NOAA/NDBC buoys and C-MAN stations (downloaded from http://www.ndbc.noaa.gov/). Wind stresses from these in situ measurements were estimated by bulk formula with neutral stability to scale the wind velocity to a standard 10 m height (e.g., Large and Pond, 1981; Blanton et al., 1989). Other wind information were acquired from the NOAA/NCEP/NARR reanalysis 10 m standard height winds (Kistler et al., 2001; Mesinger et al., 2006) available from 1979 through 2008 and downloaded from NOAA/OAR/ESRL/PSD at http://www.esrl.noaa.gov/psd/, along with the global surface (adjusted to a standard 10 m height) wind and wind stress climatologies from 8 years of QuikSCAT scatterometer data (Risien and Chelton, 2008), downloaded from http://numbat.coas.oregonstate.edu/scow/. Hourly tide gauge records from St. Petersburg, FL were downloaded from the NOAA website http://tidesandcurrents.noaa.gov/, and merged sea level anomalies (SLA) on a $1/3^\circ \times 1/3^\circ$ Mercator grid from 1992 through 2008 were obtained at the AVISO website http://www.aviso.oceanobs.com/ (Ducet et al., 2000; Le Traon et al., 2003; Pascual et al., 2006). Finally, temperature and salinity climatologies from the World Ocean Atlas 2005 (WOA05, Antonov et al., 2006; Locarnini et al., 2006) were obtained from http://www.nodc.noaa.gov/OC5/WOA05/pr_woa05.html.

Climatological monthly mean values are generally used herein to characterize the patterns of seasonal variability. We chose this technique over an annual harmonic analysis (e.g., Lentz, 2008) to describe the seasonal cycle because the currents and the winds on the WFS are asymmetric with regard to the summer (boreal) and winter (austral) half years (Liu and Weisberg, 2005b, 2007). Thus, the use of climatology, versus multiple harmonics, was deemed to be more appropriate for discussion purposes. Moreover, given the relatively long WFS moored velocity time series with 12 records exceeding 3 years, 4 exceeding 7 years, and 2 exceeding 10 years (Fig. 2), we were able to place confidence intervals about the climatological, monthly means using records of length longer than 3 years. A drawback to the climatological, monthly mean analysis is that by restricting attention to records of length exceeding 3 years (unlike the long-term mean analysis of Weisberg et al. (2009b) where records longer than 1 year were used) we must exclude most records sampled seaward of the inner shelf (nominally extending out to about the 50 m isobath).

By assuming Gaussian statistics the uncertainty for a climatological monthly mean velocity component estimate μ was derived through a standard error ε, determination computed by $\varepsilon = \sigma/\sqrt{n}$, where σ is the standard deviation of the subtidal (36 h low-pass filtered) velocity component and n is the number of independent observations in the velocity time series. Filtering was performed to remove what is mainly a deterministic portion of the variance leaving the stochastic portion as a contributor to the standard error. The number of independent observations, n, was estimated as $n = T/\tau$, where T is the record length, and τ is the decorrelation time scale. As discussed in Weisberg et al. (2009b) τ was found to be in the range of 2–4 days. To err on being conservative we used $\tau = 5$ days for either of the velocity components for all the moorings.

Table 1
Mooring information.

Mooring name	Longitude (W)	Latitude (S)	Water depth (m)	Top bin (m)	Bottom bin (m)	Start date	End date	Record length (days)
C01	82°57.00′	27°13.40′	25	4	23	13/07/1998	25/08/2001	1139
C02	82°52.20′	27°06.00′	25	4	23	13/07/1998	25/08/2001	1099
C04	84°15.00′	26°34.40′	162	15	145	25/06/2000	25/06/2001	365
C05	83°20.40′	26°57.00′	50	3	45	12/05/1999	06/12/2001	770
C06	83°00.35′	27°08.10′	30	3	27	14/09/1998	06/12/2001	1122
C07	82°13.40′	26°25.40′	10	3	8	15/09/1998	23/08/2001	1066
C08	83°49.20′	26°45.00′	78	10	60	25/06/2000	11/09/2001	443
C09	83°27.00′	27°29.20′	42	4	37	08/03/2001	25/04/2002	412
C10	82°56.47′	27°10.10′	25	3	22	14/09/1998	09/03/2008	2882
C11	82°48.00′	27°13.20′	20	3	18	13/07/1998	23/01/2009	3539
C12	83°44.20′	27°27.00′	50	3	45	05/06/1998	06/11/2007	2479
C13	83°04.20′	26°04.20′	50	4	45	01/09/1999	22/01/2009	2623
C14	83°18.00′	28°19.40′	20	4	18	24/04/2002	06/06/2008	1733
C15	82°38.40′	27°17.40′	10	3	8	14/07/1998	16/03/2009	3572
C16	84°13.20′	27°28.20′	74	5	62	22/09/2003	01/09/2006	749
C17	82°13.20′	25°15.00′	25	4	22	18/09/2003	13/01/2008	1345
C18	83°43.40′	25°01.40′	88	16	71	20/09/2003	11/01/2008	1170
C19	82°43.20′	24°37.20′	27	4	23	19/09/2003	26/11/2008	1894

3. Seasonal variation of the winds

As evident in either of the analyzed wind fields (NARR or scatterometer) or the in situ observations, the monthly mean winds over the WFS are seasonally varying (Figs. 3 and 4). Spatial variations are also observed. Over the central portion of the WFS, where most of our moored ADCP observations are located, the winds during the boreal fall, winter, and spring seasons (from October through April) tend to be northeasterly, or upwelling-favorable. During boreal summer (June through August), the winds tend to be southerly and southeasterly, or downwelling-favorable. During the transitional months (May and September), the winds have an easterly tendency, which for shallow water (e.g., <30 m isobath) is also upwelling-favorable (e.g., Li and Weisberg, 1999a; Tilburg, 2003; Liu and Weisberg, 2005a, 2007; Fewings et al., 2008). With regard to wind stress magnitude, the monthly mean winds are stronger in winter (at approximately 0.04–0.06 Pa) than in summer (at approximately 0.01–0.03 Pa), and October is the month of strongest wind stress. This seasonal variation is in agreement with previous analyses based on individual meteorological station

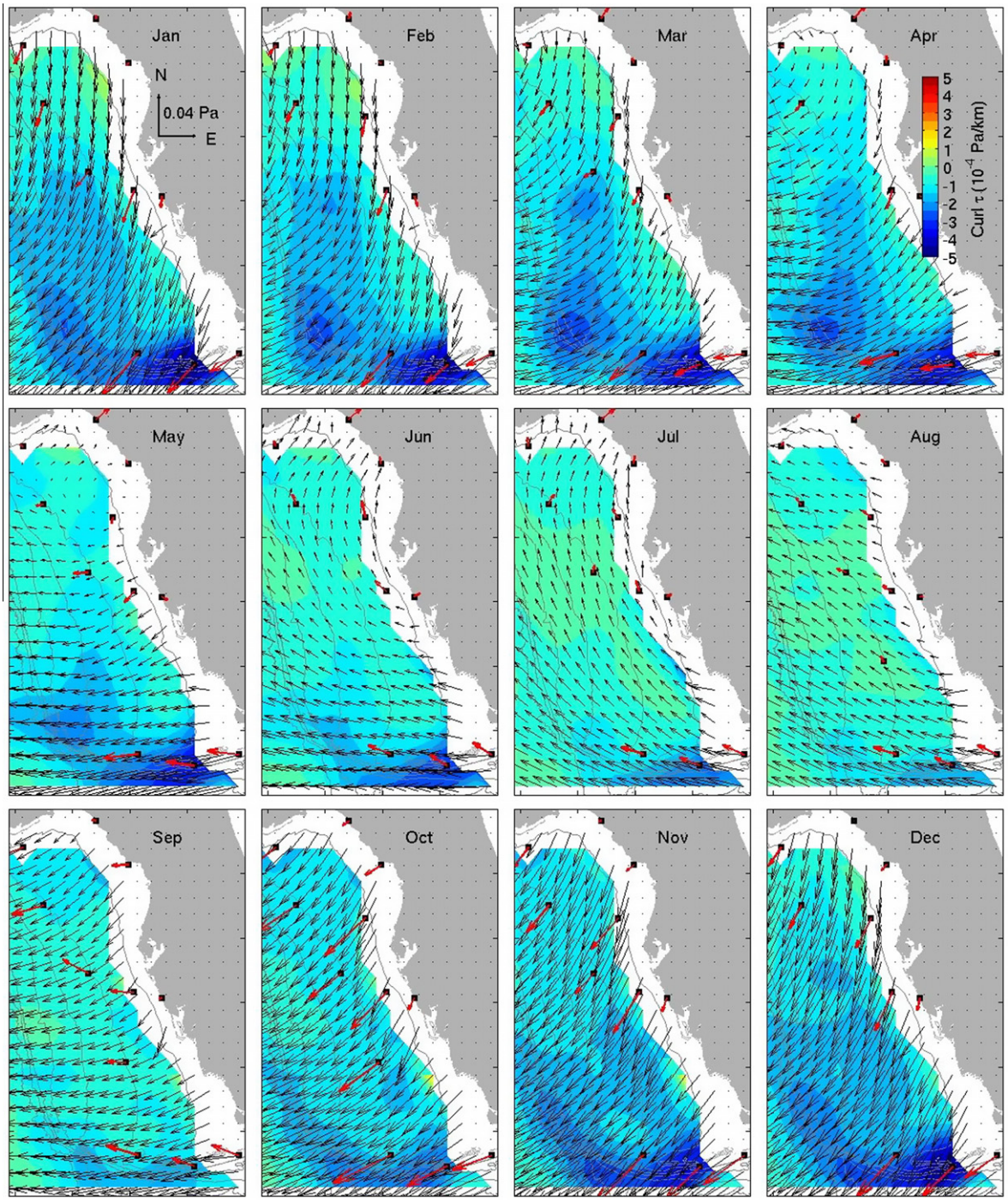

Fig. 3. Monthly mean climatology of wind stress (τ) and curl τ from the Scatterometer Climatology of Ocean Winds (SCOWs; Risien and Chelton, 2008). Also shown are monthly mean climatology of wind stress measured at University of South Florida buoys and at NDBC (National Buoy Data Center, NOAA) buoys and C-Man stations (data downloaded from http://www.ndbc.noaa.gov/). For in situ winds, only the mean values estimated from records longer than 3 years are shown.

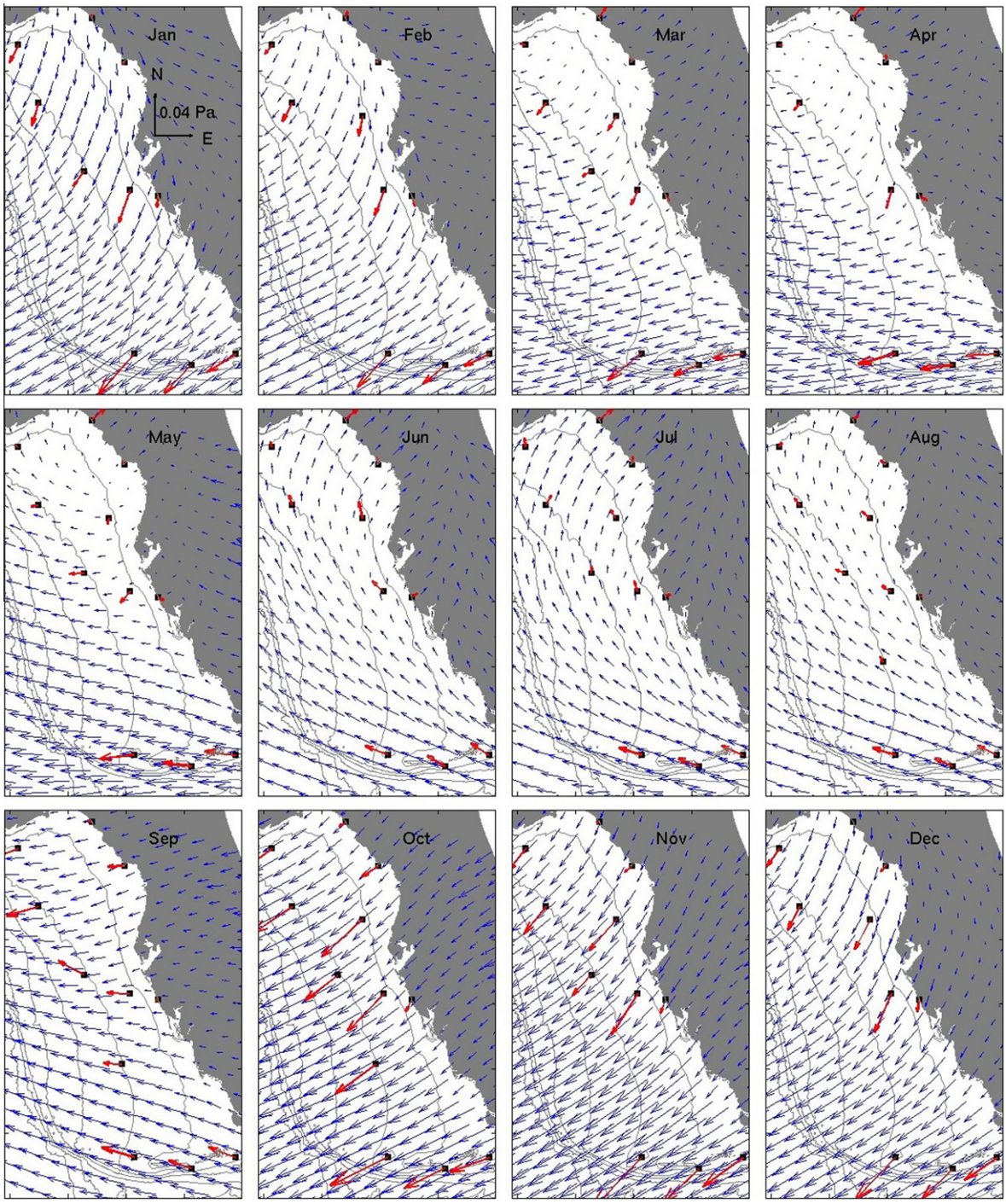

Fig. 4. Monthly mean climatology of wind stress (τ) from NCEP reanalysis product (1979–2008) overlapped with that of the in situ winds. For the latter, only the mean values estimated from records longer than 3 years are shown.

records (e.g., Virmani and Weisberg, 2003; Liu and Weisberg, 2005b, 2007).

Given the north–south extent of Florida relative to the position of the trade winds over the southern portion of the subtropical gyre, there tends to be a systematic increase in the easterly component of wind velocity from north to south. Thus, going from north to south the climatological monthly mean winds tend toward being stronger and more easterly and the seasonality tends to be less pronounced in the south because of easterlies being present year-round. Also on the basis of the trade winds, the weakest of the monthly mean winds in spring through summer are located in the north [see Smith and Jacobs (2005) for a discussion of the seasonal winds over the northern portion of the Gulf of Mexico]. These spatial variations throughout the year tend to impart a negative wind stress curl, which generally increases toward the south (Fig. 3).

The influence of increasing trade winds to the south may also help to explain previous surface drifter behaviors. By adding to the upwelling circulation, stronger easterlies in the south would contribute to the existence of the drifter trajectory forbidden zone identified by Yang et al. (1999), seen from recent observations (e.g., Price et al., 2006; Liu and Weisberg, 2011; Liu et al., 2011b) and

modeled via Lagrangian analyses (e.g., Olascoaga et al., 2008; Beron-Vera and Olascoaga, 2009).

Whereas the two different wind analyses are similar in some respects, they also exhibit differences. For example, there are 10–40° angular offsets between the observed and the satellite estimated monthly mean climatologies at some stations. Also, the satellite estimated winds are slightly larger than the model simulated winds near the coast, even with some of the near coast winds removed. This is because the scatterometer winds may be unreliable within 30 km of the coast (Perlin et al., 2004; Risien and Chelton, 2008), and the model winds may have biases near land-sea boundaries (Kara et al., 2008). Thus neither the satellite nor the model wind products adequately resolve the inner shelf wind features for the WFS. This highlights the need for sustained in situ wind observations over the coastal ocean and for assimilation of these observations in wind analysis products (e.g., He et al., 2004; Alvera-Azcárate et al., 2007; Kara et al., 2007; Chao et al., 2009). Moreover, as demonstrated by He et al. (2004), inadequate winds are a major source of error in simulations of the coastal ocean circulation. These differences between the wind stress products and the in situ observations notwithstanding, both the seasonal variability and the spatial heterogeneity of the monthly mean climatological wind stresses are seen in all three wind analysis sets, lending credence to the overall pattern of seasonal wind variability as characterized herein.

4. Seasonal variations in the WFS circulation

4.1. The depth-averaged currents

4.1.1. Monthly mean climatology

Depth-averaged velocity vectors are estimated by trapezoidal integration of the 1 m binned ADCP data. These results are very similar to averages formed by linearly extrapolating the velocity profile to the surface and the bottom to fill in those data gaps. The resulting climatological, monthly mean, depth-averaged currents on the WFS (Figs. 5 and 6) tend to be southeastward directed (along-shore and down-shelf) from October to through April and northwestward directed (along-shore and up-shelf) from June through September. Fig. 5 shows the spatial patterns and Fig. 6 shows the temporal variations along with the standard errors of the mean estimates. Over the inner shelf, these monthly mean currents are also of larger magnitudes from fall to spring months (0.02–0.12 m s^{-1}) than in summer months (0–0.06 m s^{-1}), with the strongest currents (0.10–0.12 m s^{-1}) occurring from October to January. These correspondences in magnitudes and directions between the evolution of the depth-averaged current patterns (Fig. 5) and the wind patterns (Figs. 3 and 4) suggest that local wind forcing is a major contributor to the seasonality of the WFS's inner shelf circulation (e.g., Weisberg et al., 2001, 2005, 2009b; He and Weisberg, 2002, 2003; Liu and Weisberg, 2005a, 2007).

Seasonally varying spatial structure is also observed across the inner shelf. Note that for the central region of the WFS, where data are sufficient to resolve the spatial structure, a southeastward coastal jet tends to have a velocity core of amplitude 0.10–0.12 m s^{-1} positioned between about the 25–30 m isobaths in fall through spring, whereas a weaker northwestward coastal jet with velocity amplitude of 0.05–0.06 m s^{-1} is positioned between about the 20–25 m isobaths in summer (June, July, and September). This asymmetry in the seasonal reversal of the inner shelf circulation is consistent with the long-term mean flow findings of Weisberg et al. (2009b).

Unlike the inner shelf, the seasonality of the depth-averaged currents farther offshore is not as well defined. Whereas the climatological, monthly mean, depth-averaged currents along the 50 m isobath (moorings C12 and C13) are generally down-shelf from October through June (Figs. 5 and 6), similar to the other inner shelf currents, these currents are either weak or of ill-defined direction from July through September, (Figs. 5 and 6), also consistent with the long-term mean flow findings.

Observations from moorings at the southern end of the WFS (C18 and C19) do not exhibit any obvious seasonality in depth-averaged currents (Fig. 5). This is likely due to the close proximity of these moorings to the shelf break where the currents are influenced by the proximity of the Loop Current and its eddies (e.g., Niiler, 1976; Molinari et al., 1977; Huh et al., 1981; Paluszkiewicz et al., 1983; He and Weisberg, 2002; Vukovich, 2007), which can overwhelm the effects of local wind forcing. Episodically, if the Loop Current encounters shallow isobaths near the Dry Tortugas even the inner shelf currents are affected (e.g., Weisberg and He, 2003). Similarly, while the currents at mooring C17 (25 m isobath) are consistent with the upwelling patterns on the inner shelf during fall and winter months (October–March), they are weak and ill defined in spring and summer months.

4.1.2. Wavelet analysis of the depth-averaged currents

Wavelet power spectra are useful for examining the temporal evolution of the variance distributions across frequency space. Here we use a wavelet analysis to examine the variance evolution for the along-shelf component of the depth-averaged currents and the partition of variance between synoptic and seasonal time scales.

Prior to wavelet analysis all of the velocity time series were low-pass filtered to remove oscillations at time scales shorter than 48 h, then subsampled at a 12-h interval, and rotated to their principal axis directions to acquire the along-shelf (principal axis) components. The three longest records available for such analyses are from moorings C15, C11 and C10, located on the 10, 20 and 25 m isobaths, respectively. Mooring C11 was chosen to represent the inner shelf because it has a long record and a central location. The C11 data gap (Fig. 2b) was filled up by inference from the adjacent moorings using a linear regression analysis. Mooring C12, located at the 50 m isobath, was chosen to represent a station farther offshore. C12 data gaps were also filled by linear regression analyses using data from moorings from C05 and C13, both on the 50 m isobath. Remaining short data gaps were then filled using other adjacent moorings, with preference in the order of C09 and C10. Given these preconditioned time series the Torrence and Compo (1998) wavelet toolbox was used with the wavelet power spectrum rectification discussed by Liu et al. (2007).

The wavelet power spectra for the along-shelf, depth-averaged currents at moorings C11 and C12 identify four features. First, the along-shelf circulation variance is separable between synoptic and seasonal time scales, with the variance at synoptic scale (here inclusive of 2–16 day periodicities) exceeding that at the seasonal scale (Fig. 7). This is consistent with wind forcing and in agreement with previous inferences (e.g., Liu et al., 2007; Weisberg et al., 2005). Second, whereas the C11 wavelet power on seasonal time scale is statistically significant at 90% confidence throughout the 10 years, the seasonal time scale variance at C12 is not, i.e., the seasonal variation is robust at the shallow site, but not at the offshore site. This agrees with the previous inference (Figs. 5 and 6) that the seasonality of the central WFS circulation decreases seaward from the center of the inner shelf. Third, the wavelet power spectra show a seasonal modulation in the along-shelf velocity component synoptic scale variability at the offshore site, which is not as obvious at the shallower, inner shelf site. This cannot be explained on the basis of wind forcing alone because the winds at the two sites are similar (for instance, Cragg et al. (1983) argues that the coherence length scale for the synoptic scale wind fluctuations is about 200 km). Such seasonal modulation differences with offshore

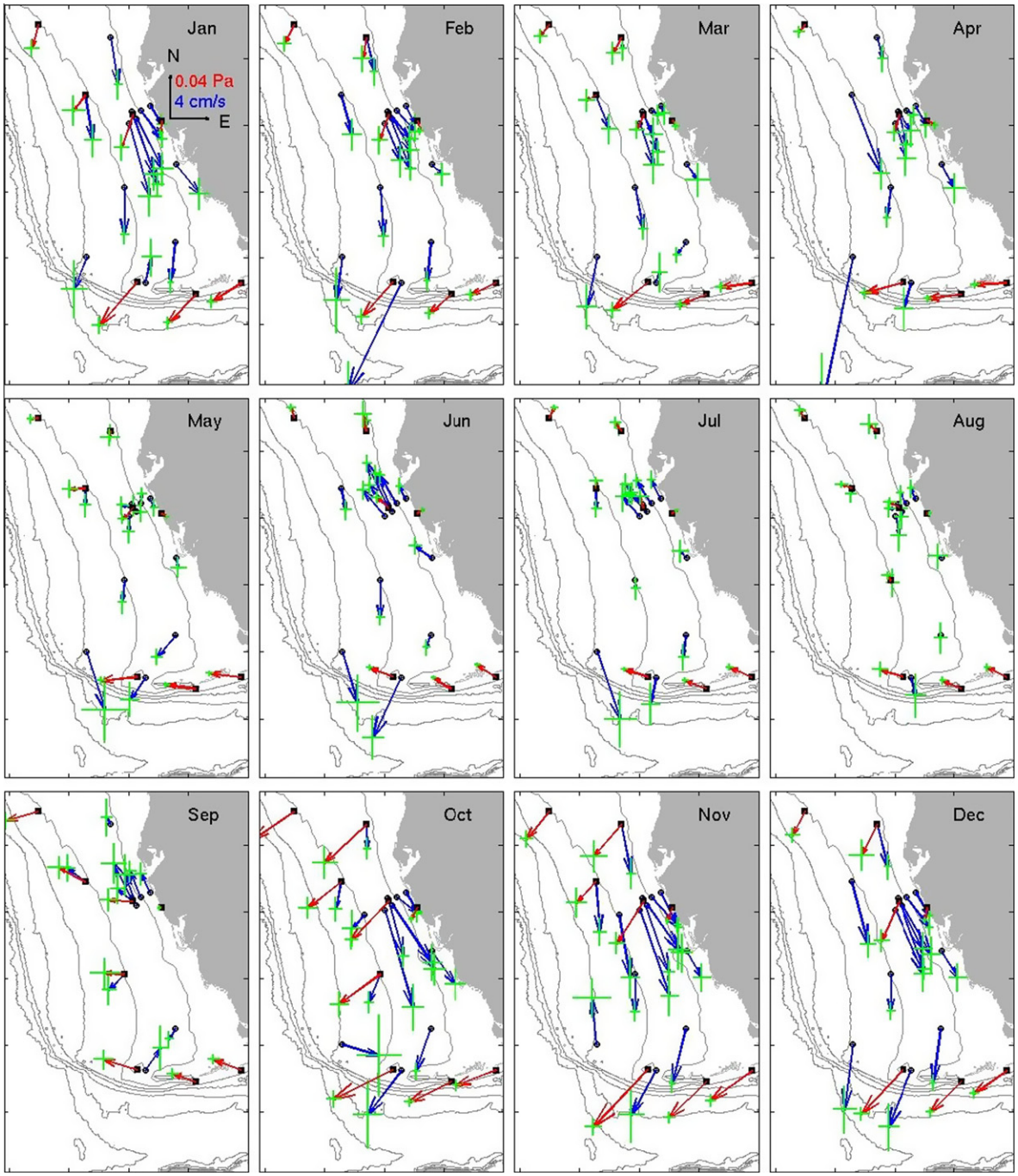

Fig. 5. Monthly mean climatology of wind stress (red) and depth-averaged velocity vectors (blue). The standard errors ε (green) of the mean values μ are shown as crosses ($\mu \pm \varepsilon$) at the arrow heads. Only the mean values estimated from records longer than 3 years are shown.

distance are consistent with seasonal variations in baroclinicity as previously postulated by Weisberg et al. (1996) and later demonstrated by He and Weisberg (2002). Thus the seasonality of the WFS circulation is by a combination of wind and buoyancy forcing, with buoyancy entering both by differential heating in the across-shelf direction (due to water depth changes) and fresh water inflows to the inner shelf via local rivers and to the middle and outer shelf regions by the Mississippi River and by the rivers located along the Florida Panhandle in the north. Fourth, the wavelet power spectra show some intraseasonal variations, especially at the offshore site (Fig. 7b). Such intraseasonal to interannual modulations may be related to the Loop Current eddy shedding cycle (e.g., Sturges and Leben, 2000; Carnes et al., 2008; Alvera-Azcárate et al., 2009; Hallock et al., 2009) and with limited duration interactions of the Loop Current with the shelf slope (e.g., Weisberg and He, 2003; He and Weisberg, 2003). Such behaviors warrant further study, but are beyond the scope of our present analyses.

4.2. Vertical structure

4.2.1. Velocity vector veering with depth

Vertical profiles of the monthly mean velocity vectors across the inner shelf (Figs. 8 and 9) exhibit seasonal variation as previously seen in the vertical averages. Upwelling favorable current

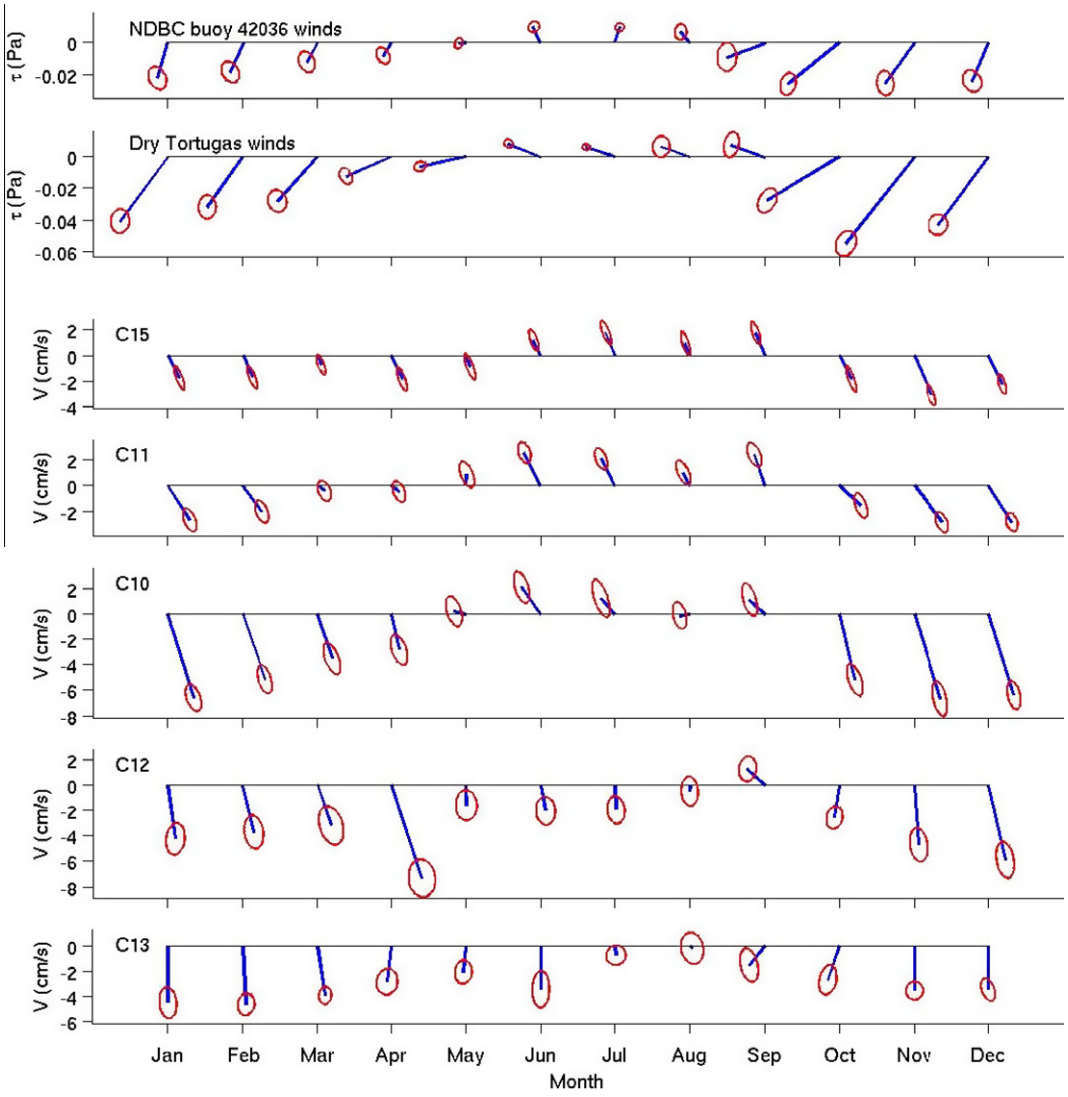

Fig. 6. Monthly mean wind stress (top two panels) at NDBC buoy 42036 over the northern WFS and Dry Tortugas on the southern WFS, and monthly mean depth-averaged velocity vectors (bottom five panels) at the sites (C15, C11, C10, C12 and C13) with record length longer than 7 years. The uncertainties are estimated as the standard errors but from the principal axis currents rather than from the standard deviations of the east- and north-components.

structures are evident from October through April, whereas downwelling favorable current structures are evident from June through September. During upwelling months the southeastward current vectors systematically rotate to the left from surface to bottom, i.e., the near-surface currents have a seaward directed component, and the near-bottom currents have a landward directed component. The near-surface and the near-bottom currents also have about the same magnitudes, 0.06–0.12 m s^{-1}. During downwelling months the northwestward current vectors also exhibit left-hand rotation from surface to bottom, i.e., the near-surface currents tend to have a small landward directed component, and the near-bottom currents have a seaward directed component. However, during the downwelling season the near-surface currents tend to be much stronger than the near-bottom currents, 0.06–0.12 m s^{-1} versus 0.02–0.03 m s^{-1}. The asymmetries between the monthly mean upwelling and downwelling current structures are similar to those found for the subtidal time scales (e.g., Weisberg et al., 2005; Liu and Weisberg, 2005b, 2007).

Further offshore at the 50 m isobath, where the inner shelf begins to transition to the middle shelf, the vertical veering of the monthly mean velocity vectors with depth is less pronounced or even ambiguous (Figs. 8 and 9). During most of the upwelling season (November through April), the velocity vectors do not veer as much (relative to more shoreward locations), and the maximum amplitudes are often at subsurface levels. From May through October, the monthly mean vectors have magnitudes that are often less than their standard errors; hence the monthly mean values at specific depths may not be robust.

The most ill-defined of these monthly mean velocity vectors are those located near the southern end of the WFS (C18 and C19). Large variability there is due to the near shelf break proximity of these two moorings and hence Loop Current and eddy interaction influences that tend to overwhelm the seasonal variations, at least in so far as the record lengths presently available.

4.2.2. Vertical profiles of the across- and along-shelf components of velocity

This section examines the climatological monthly mean vertical profiles of across- and along-shelf components of velocity for the three moorings with the longest record lengths distributed over the inner half of the inner shelf: C15, C11, C10 at the 10 m, 20 m, and 25 m isobaths, respectively. The along-shelf directions, determined from the principle axes (for instance see, Emery and Thomson, 2001) of the C15, C11, C10 subtidal depth-averaged velocity

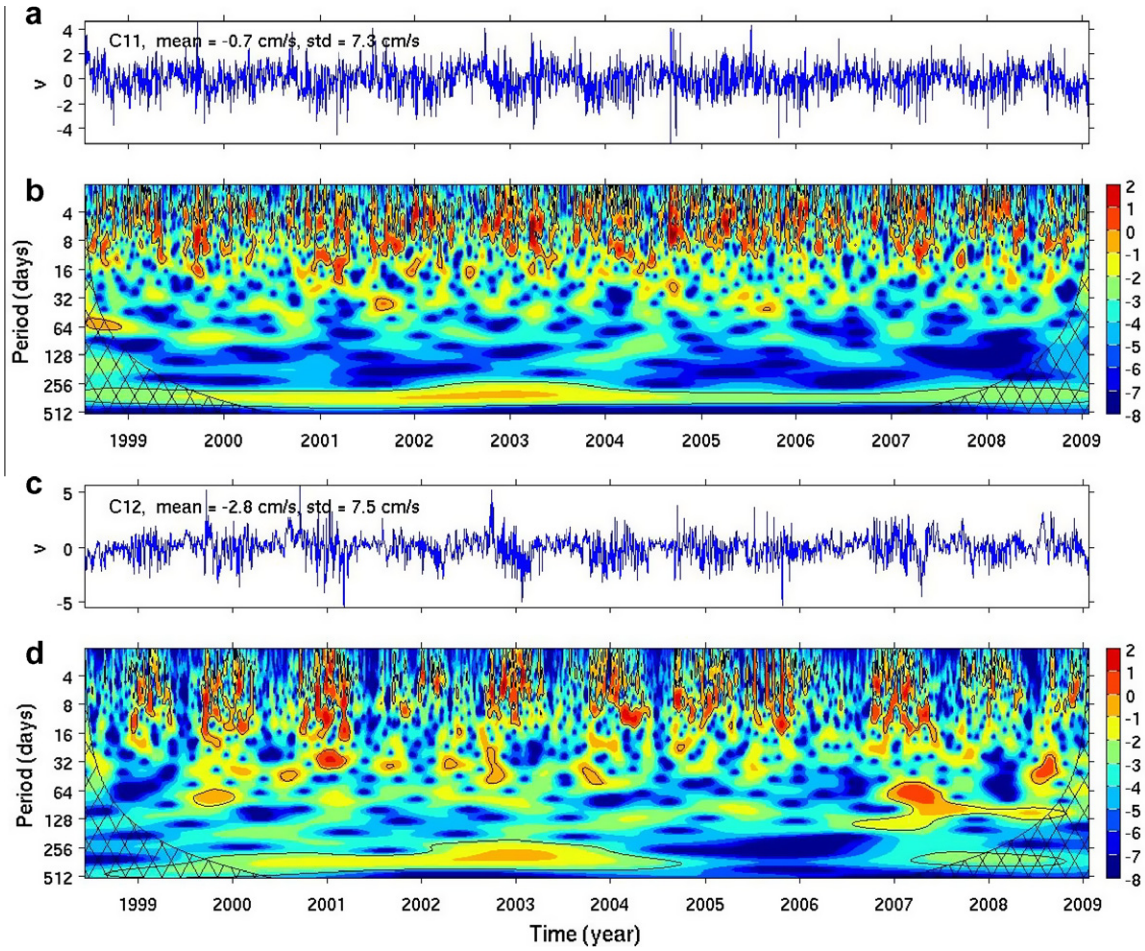

Fig. 7. Wavelet analyses of the depth-averaged along-shelf velocity of moorings C11 (a and b) and C12 (c and d) on the West Florida Shelf. Time series of velocity are detided, 48-h low-pass filtered, 2-h subsampled, and normalized (minus the mean and divided by the standard deviation) prior to wavelet analyses. Wavelet power spectra are shown in base 2 logarithm. The regions of greater than 90% confidence are shown with black contours. Cross-hatched regions on either end indicate the "cone of influence," where edge effects become important.

vectors, are 29.8°, 36.1° and 29.7° anticlockwise from the north, respectively, and aligned approximately parallel to the local isobaths (Fig. 2).

At the 10 m site (C15), the climatological monthly mean across-shelf currents show a distinctive two-layer structure from September through April (Fig. 10a). The upper layer currents are directed offshore, and lower layer currents are directed onshore, constituting a coastal upwelling circulation. The largest across-shelf component magnitudes (0.01 m s^{-1}) occur in October and November, corresponding to the largest magnitudes of the climatological monthly mean upwelling favorable wind velocity vectors (Fig. 3). Note that the top- and bottom-most two to three meters of the water column are not observed by the ADCPs so the magnitude of the largest across-shelf component may be underestimated. The across-shelf current structures are more complicated at the 20 m and the 25 m sites (C11 and C10). The across-shelf velocity component magnitudes increase at these farther offshore locations, and the directions, at times, do not convey a simple two layered structure (Fig. 10c and e). This demonstrates that even across the inner shelf the currents must be considered as being fully three dimensional (e.g., Li and Weisberg, 1999a). At none of these three sites do we see what could be interpreted as a simple balance between offshore and onshore directed flows. In other words mass cannot be closed within a two-dimensional framework, rendering two dimensional models (across-shelf and depth) irrelevant to the nature of WFS circulation. Accelerating or decelerating alongshore currents are required for mass balance. Such a result is not surprising in view of the convergence of isobaths that occurs in this region, and behaviors like these are generally seen in numerical model experiments, e.g., Weisberg et al. (2000, 2001).

The climatological monthly mean along-shelf currents (Figs. 10b, d and f) tend to vary in a manner consistent with the across-shelf currents and wind. Months with upwelling favorable winds exhibit flows from down-coast from northwest to southeast, and conversely for months with downwelling favorable winds, consistent with the local wind seasonal variation. Whereas the down-coast along-shelf component magnitudes appear to increase offshore to the 25 m isobath during the upwelling season, this is not the case for the up-coast directed flows during the downwelling season. Such asymmetry is consistent with what is observed for the responses of the shelf to synoptic scale variability (e.g., Weisberg et al., 2001; Liu and Weisberg, 2005a, 2007).

5. Seasonal variation of the sea surface heights

Liu and Weisberg (2007) determined the portion of the coastal sea surface height (SSH) fluctuations on the WFS that could be attributed to the dynamical responses of the inner shelf circulation to the along-shelf and across-shelf winds and buoyancy. A residual at the 50 m isobath, after subtracting these dynamical responses that were estimated by integrating their slopes landward from the 50 m isobath, was found to be coherent with a satellite

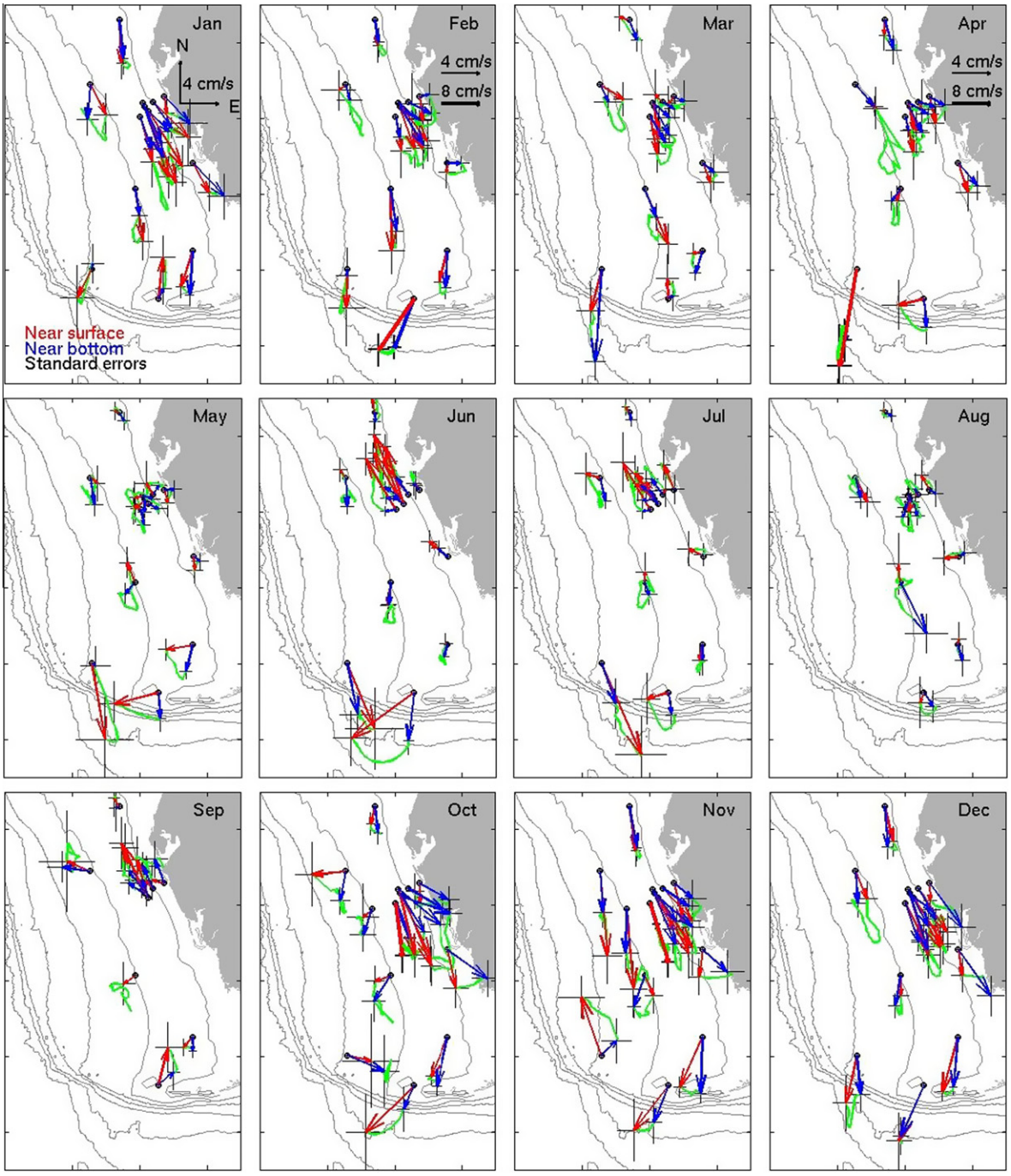

Fig. 8. Monthly mean near-surface (red) and near-bottom (blue) velocity vectors. The monthly mean velocity vector vertical profiles are shown as green lines connecting the arrowheads of the near-surface and near-bottom velocity vectors. The standard errors ε of the mean values μ are shown as crosses ($\mu \pm \varepsilon$) at the arrow heads for near-surface currents. Only the mean values estimated from records longer than 3 years are shown.

altimetry derived sea surface height anomaly at the 50 m isobath. A portion of this anomaly was attributed to the dynamic height variations due to observed temperature and salinity variations, but the origin of this residual sea level variability at the 50 m isobath remained to be determined. This section expands upon those previous analyses by using longer time series and SSH analyses from the larger scale Gulf of Mexico.

5.1. Coastal sea level

Coastal SSH variations are immediately identifiable in a 20 year tide gauge record sampled at St. Petersburg, FL. To focus in on interannual to seasonal and synoptic variations, this time series was first preconditioned as follows. We de-tided by removing the four major tidal constituents, M2, S2, O1 and K1 [using the T_Tide harmonic analysis software of Pawlowicz et al. (2002)]. We then low-pass filtered (with a 48 h cut-off) and adjusted for the inverted-barometer effect (using the sea level pressure records from either the NDBC buoy 42036 or other proximate C-MAN stations). The results, upon subsampling every 12 h, are shown in Fig. 11a. After removing the temporal mean and normalizing with the standard deviation, this preconditioned SSH record was subjected to a wavelet analysis as shown in Fig. 11b.

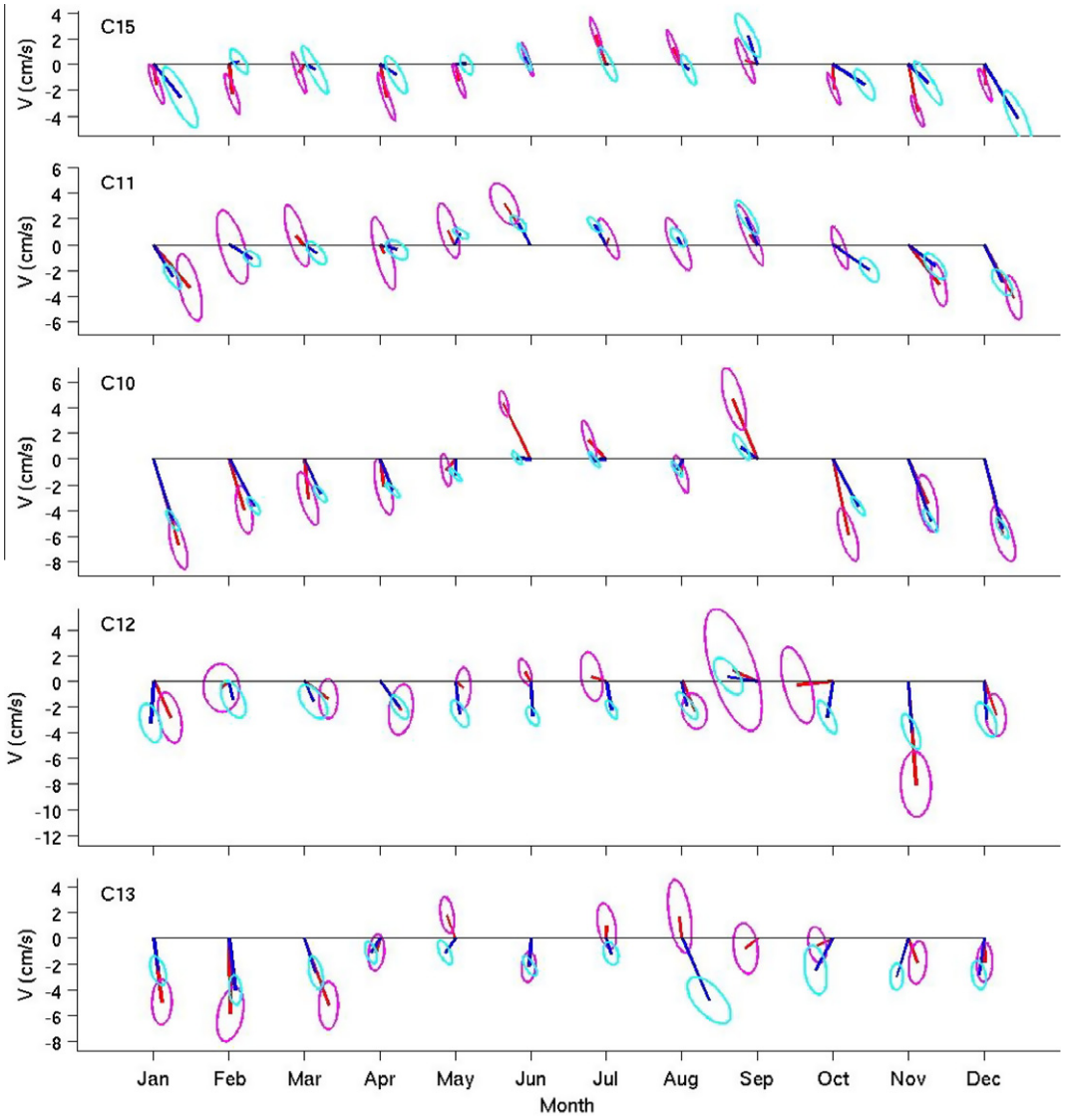

Fig. 9. Monthly mean near-surface (red) and near-bottom (blue) velocity vectors at the sites (C15, C11, C10, C12 and C13) with record length longer than 7 years. The uncertainties are estimated as the standard errors but from the principal axis currents rather than from the standard deviations of the east- and north-components. (For interpretation of the references to color in this figure legend, the reader is referred to the web version of this article.)

As in Fig. 1, the SSH time series shows that the synoptic scale variations, plus a few outliers due to tropical storms, exceed the interannually modulated seasonal variations, imparting a combined standard deviation of 0.13 m. The partition of SSH variance and its modulation are more evident in the Fig. 11b wavelet power spectrum, where, similar to that of the along-shelf component of velocity (Fig. 7), there exists a separation between variances at the synoptic weather band and at the seasonal time scale (Fig. 11b), along with an interannual modulation. What differs between the SSH and the along-shelf component of velocity is that the seasonal and synoptic scale variances are comparable for SSH, which is not the case for the along-shelf component of velocity, i.e., the seasonal variation of the coastal sea level is proportionately larger than that of the along-shelf component of velocity.

Another feature of the wavelet power spectrum for coastal SSH is the seasonal modulation of the synoptic scale variations, i.e., the spectral values are larger in winter than in summer. Liu and Weisberg (2007) showed that the synoptic variations in coastal SSH derive mainly from three sources: the barotropic and baroclinic geostrophic along-shelf velocity component responses to the along-shelf wind stress and the frictional response to the across shelf wind stress. Given that the seasonal cycle of SSH is proportionately larger than that of the inner shelf, along-shelf velocity component (Fig. 7b), we hypothesize that the larger SSH seasonal cycle must be partially of offshore Gulf of Mexico origin.

5.2. Offshore sea level

Sea level pressure adjusted SSH variations arise through two contributions, one dynamic, the other static. Dynamic SSH variations, either barotropic (density independent under an incompressibility assumption) or baroclinc (density dependent) arise from mass re-distributions by geostrophic adjustment, e.g., the sea level slope across the Loop Current, or the wind-driven Ekman-geostrophic spin up of the inner shelf. Static SSH variations arise by heating and cooling alone without ocean dynamical adjustment, i.e., the uniform rise and fall of sea level by static steric effects after the gradients have adjusted geostrophically. On seasonal and longer time scales, both dynamic and static effects may be important, but with only the dynamic effects being realizable within volume conserving ocean circulation models.

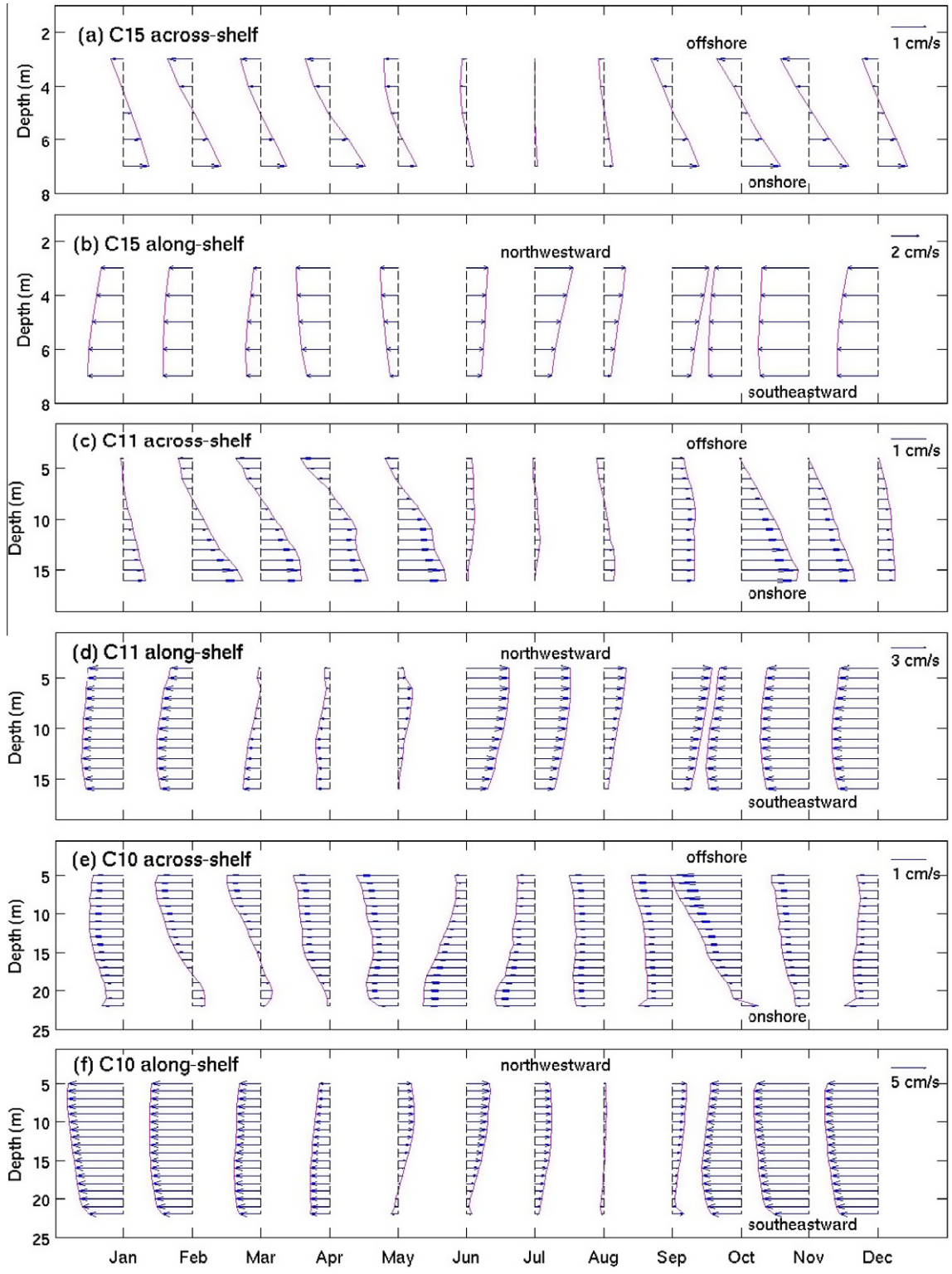

Fig. 10. Monthly mean across- and along-shelf velocity profiles at moorings C15, C11, and C10 (on 10, 20 and 25 m isobaths, respectively). Note that the velocity scales of the along-shelf component are different for the three stations.

5.2.1. Steric height in Gulf of Mexico deep water area

We estimate the static steric contribution to coastal SSH imposed by the deep Gulf of Mexico by spatially averaging the steric height variations calculated from a monthly mean climatology of water temperature and salinity (World Ocean Atlas). To isolate the deep ocean from additional coastal ocean contributions we restrict the analysis to Gulf of Mexico regions with water depths in excess of 600 m, i.e., the continental slope and the abyss. Spatial averaging across the entire deep Gulf of Mexico eliminates dynamical effects due to the adjustments to gradients in temperature and salinity. Fig. 12a and b show the climatological results. Note that the analysis considers the upper 600 m of the water column where most of the variation occurs, and to further quantify this we broke this region into six separate 100 m bins, i.e., 0–100 m, 100–200 m

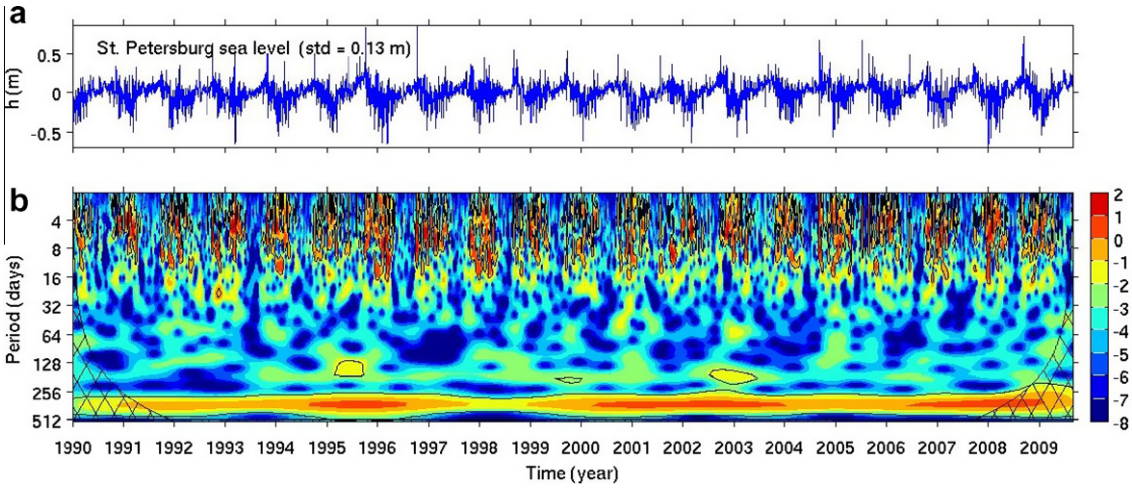

Fig. 11. Wavelet analysis of the St. Petersburg sea level. Time series of sea level are detided, 48-h low-pass filtered and 12-h subsampled, adjusted for inverted-barometer effect, and normalized (minus the mean and divided by the standard deviation) prior to wavelet analyses. Wavelet power spectra are shown in base 2 logarithm. The regions of greater than 90% confidence are shown with black contours. Cross-hatched regions on either end indicate the "cone of influence," where edge effects become important.

and so on. We also calculated the overall steric height across each of these bins (Fig. 12a) and then the seasonal anomaly in steric height by subtracting out the annual mean for each bin (Fig. 12b). The monthly mean steric height contributions in the top six 100-m layers are shown in Fig. 12. The monthly mean steric height contributions from the upper 100 m layer range from about 0.28 m to 0.39 m with a 12-month mean value of about 0.34 m. These mean steric height contributions decrease with increasing water depth, with values of 0.20, 0.14, 0.12, 0.10 and 0.09 m in the next five successive 100 m layers, respectively. After subtracting the annual mean values from the monthly mean steric heights, the climatological monthly mean steric height anomalies are given in Fig. 12b. These range from −0.062 to +0.055 m, −0.009 to +0.009 m, −0.007 to +0.005 m, for the first three 100 m bins, respectively. Thus it is the upper 100 m layer that contributes the most to the static steric height variations of the deep Gulf of Mexico, and this projects a seasonal cycle onto the shelf of range approximately equal to 0.12 m with the lowest value in February and the highest value in August.

5.2.2. Satellite altimetry over the deep Gulf of Mexico

A similar analysis may be performed using satellite altimetry. Using the gridded AVISO sea level anomaly (SLA) data for the Gulf of Mexico region: 95°W–81°W, 24°N–30°N for depths in excess of 200 m, we spatially averaged to reduce dynamics effects and binned the spatially averaged anomalies by month to produce a

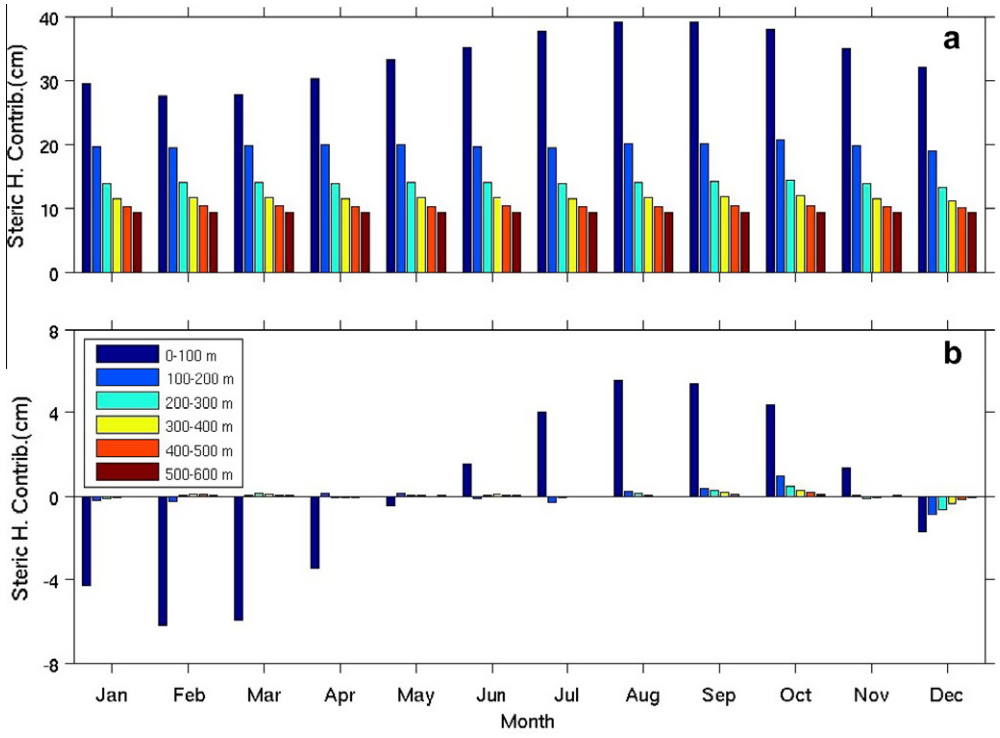

Fig. 12. Steric height contributions of the upper water layers estimated from the monthly mean climatology of temperature and salinity: (a) monthly mean steric height contributions of the top 6 100-m layers, (b) anomaly of steric height contribution.

monthly mean climatology. These results from satellite altimetry are shown together with the previous results by static steric height anomaly (over the layers 0–100 m and 100–200 m of the water column) in Fig. 13. Similar to the static steric height contributions of the upper ocean, the SLA exhibits seasonal variation with about the same amplitude, but with about a one month phase shift, i.e., the SLA lags the steric height anomaly by about a month with the highest value in October and the lowest value in March. Given that the two data sets derive from different time intervals we cannot comment on the origin of the time lag. The main result is that both the climatological static steric height and the climatological SLA have nearly the same seasonal cycle range, some 0.12 m.

5.3. Local and offshore contributions to the coastal sea level seasonal variation

How do the static steric findings comport with the monthly mean climatology of the coastal sea level at St. Petersburg, FL? The results are shown over plotted in Fig. 14, along with the sea level pressure climatology. The coastal sea level is highest in September and lowest in January. After adjusting for the inverse barometer effect the coastal sea level range is reduced by about 0.06 m, and the minimum is shifted to February, putting the two sea level anomaly time series in phase. The adjusted coastal sea level ranges from around −0.08 to 0.1 m, which is somewhat larger than what is accounted for by the deep Gulf of Mexico.

Might this difference between coastal and offshore sea level be due to local effects? Note that the monthly mean climatology for winds over the central portion of the WFS show upwelling and downwelling seasons, which, despite small phase shifts would tend to set sea level up from fall to spring and down from spring to fall. So both local wind (and atmospheric pressure) forcing and offshore steric effects contribute to coastal sea level as observed at St. Petersburg, FL.

5.4. Across-shelf sea level gradient relative to along-shelf component of velocity

Given the Section 5.3 findings, are these consistent with the observed seasonal cycle in the along-shelf component of velocity? Consider the difference between the monthly mean climatologies of St. Petersburg, FL (inverted barometer adjusted) coastal sea level (ζ_{coast}) and the Gulf of Mexico deep ocean sea level (ζ_{GOM}) averaged over the region with depths >200 m, and assume that these monthly mean differences are indicative of the sea level, (Fig. 15a), across the width of the inner shelf. Using an inner shelf width of approximately L = 100 km (i.e., from the coast to just beyond the 50 m isobath off Sarasota, FL), a Coriolis parameter $f = 0.64 \times 10^{-4}\ s^{-1}$ and an acceleration of gravity $g = 9.8\ m\ s^{-2}$, the monthly mean along-shelf geostrophic velocity, v_g may be estimated as $v_g = g(\zeta_{coast} - \zeta_{GOM})/(fL)$. For comparison, we composited a monthly mean, depth-averaged, along-shelf component of velocity climatology from moorings at depths of 50 m or less and with record lengths longer than 3 years (Fig. 5) by simply averaging the available monthly mean velocity component climatologies. We then subtracted the annual mean to produce an anomaly time series for comparison with the sea level climatologies, which already have zero annual mean (Fig. 15b). Both the sea level estimated geostrophic and the observed velocity component anomalies show a similar seasonal cycle. That is to say, on seasonal time scale, the shelf-wide along-shelf currents are approximately in geostrophic balance across the inner shelf.

Mitchum and Sturges (1982) provided a similar analysis for fluctuations over synoptic weather time scales, but assuming zero sea level change near the shelf break. Had we made a similar assumption in our seasonal time scale analysis we would have found a larger mismatch between estimated and observed climatologies (Fig. 15b). Hence for this and other important deep-ocean coastal ocean interactions (e.g., Weisberg and He, 2003) it is important to study the coastal ocean as a complete system, including its interactions with the deep-ocean, versus in isolation.

6. Discussion and summary

Sustained observations of currents using moored acoustic Doppler current profilers for the period spanning 1998–2009, plus various ancillary data, facilitated an examination of the seasonal cycles in WFS circulation and sea level. Building upon previous WFS seasonal variability inferences (e.g., Tolbert and Salsman, 1964; Yang and Weisberg, 1999; He and Weisberg, 2002, 2003; Weisberg et al., 2005; Liu and Weisberg, 2005b, 2007; Ohlmann and Niiler, 2005; Carlson and Clarke, 2009; Dzwonkowski and Park, 2010), and differing from some of these, we find that the WFS possesses a statistically robust seasonal cycle, which varies across the shelf and which also derives, in part, from the deep Gulf of Mexico. Over the (dynamically defined) inner shelf the seasonal variation of the circulation is pronounced and in response to local forcing. The inner shelf circulation is generally upwelling favorable from fall through spring (~October to April) and downwelling favorable in summer (~June–September). The upwelling circulations also tend to be larger than the downwelling circulations owing to asymmetries in both the seasonal wind stress and the coastal ocean response. Toward the offshore extent of the inner shelf and seaward from the 50 m isobath, baroclinic effects, in part due to deep

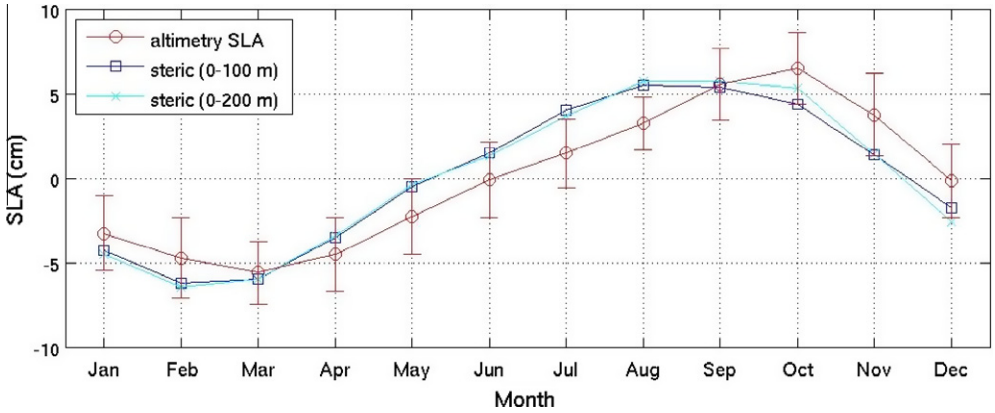

Fig. 13. Monthly mean steric height contributions of the top 100 and 1000 m water layers and sea level anomaly (SLA) of the Gulf of Mexico (>200 m) from satellite altimetry. The standard deviations of the SLA are shown as error bars.

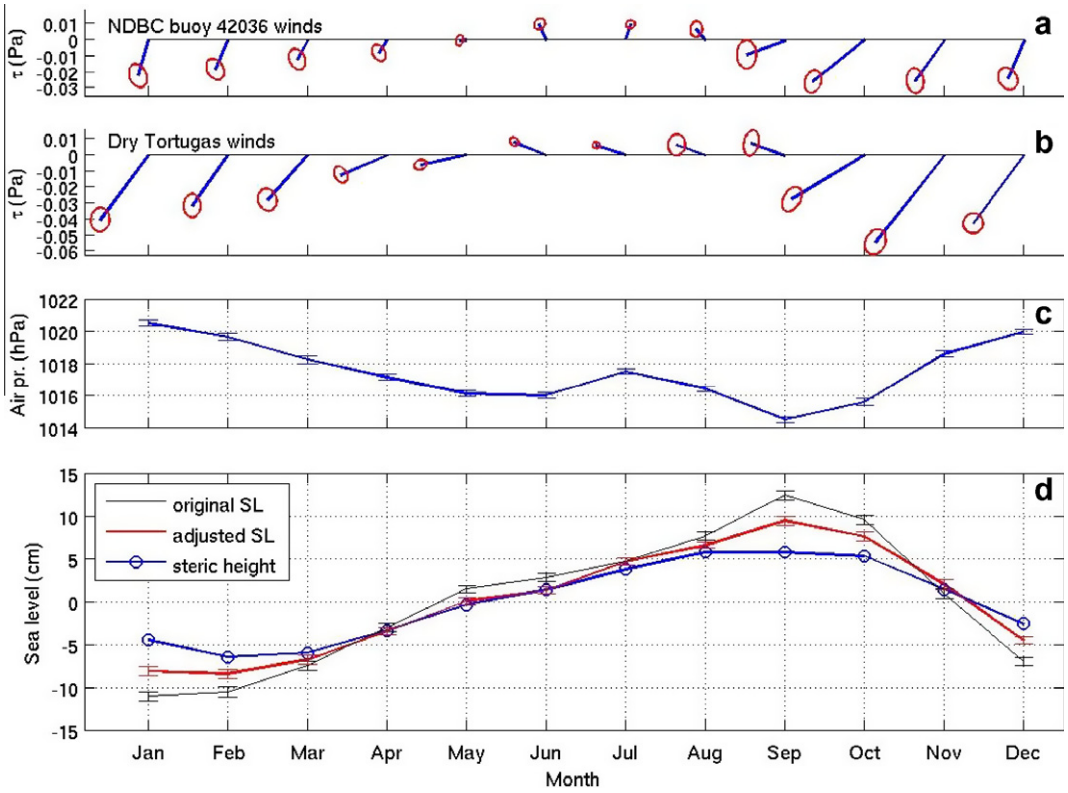

Fig. 14. Monthly mean climatology of wind stress (same as those in Fig. 6), air pressure and sea level on the WFS. (a) Wind stress at NDBC buoy 42036 over the northern WFS, (b) wind stress at Dry Tortugas on the southern WFS, (c) air pressure at NDBC buoy 42036, (d) original and air pressure adjusted sea level at St. Petersburg, and steric height (upper 200 m layer) in the Gulf of Mexico deep (>200 m) area. The standard errors are shown as error bars or ellipses.

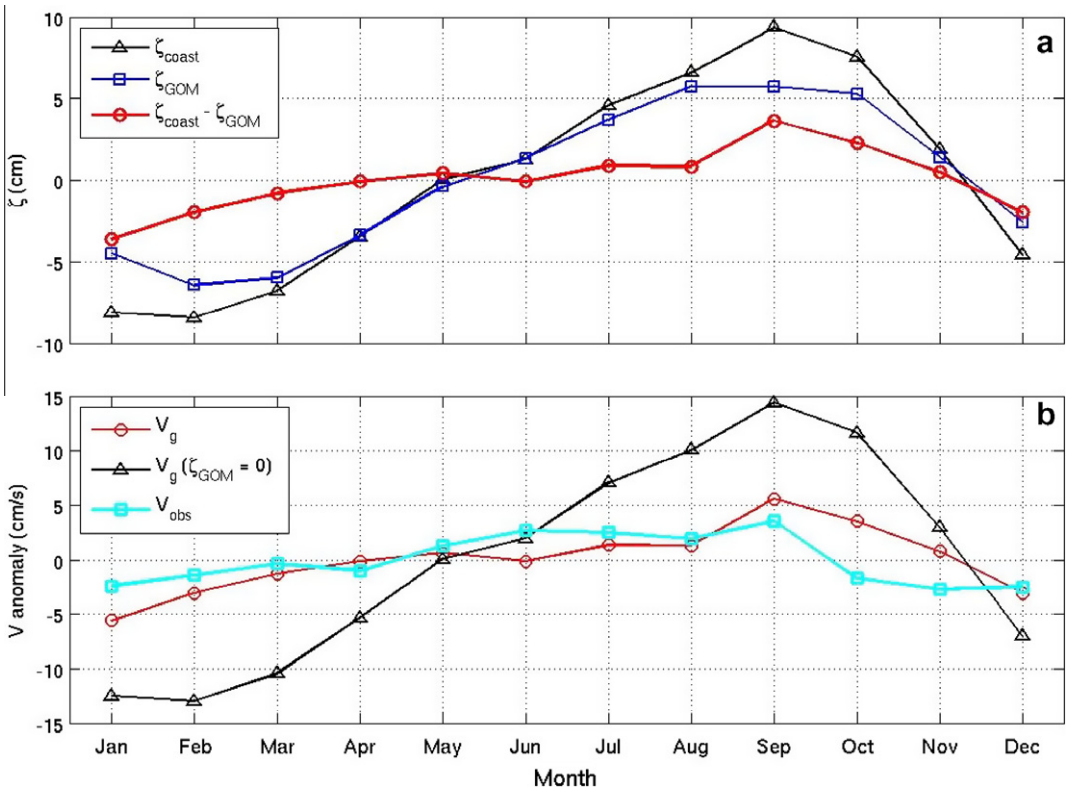

Fig. 15. (a) Monthly mean inverted barometer adjusted sea level at St. Petersburg (ζ_{coast}), monthly mean static steric height averaged over the Gulf of Mexico for depths >200 m (ζ_{GOM}), and their difference ($\zeta_{coast} - \zeta_{GOM}$). (b) Monthly mean along-shelf geostrophic velocity (V_g) using ($\zeta_{coast} - \zeta_{GOM}$) and a 100 km length scale representative of the inner shelf (the coastline out to just beyond the 50 m isobath), monthly mean along shelf velocity component anomaly averaged for moorings at depths of 50 m or less (V_{obs}), and the along-shelf geostrophic velocity using ζ_{coast} and assuming no static steric adjustment to sea level offshore (V_g ($\zeta_{GOM} = 0$)).

ocean interactions and increased stratification with increased depth, begin to obscure the mostly wind driven seasonal cycle of the inner shelf, making the seasonal cycle less pronounced offshore. Over the outer shelf the episodic impacts of the deep ocean through the Gulf of Mexico Loop Current and eddy interactions become controlling over the effects of local forcing.

In contrast with that of the WFS currents, the seasonal variation of sea level is pronounced across the entire shelf from the coast to the shelf break and beyond. A portion of this seasonal variability derives from the deep Gulf of Mexico through static steric height changes owing to seasonal heating and cooling. This deep ocean cycle in sea level exhibits its lowest value in February and its highest value in August, and most of this order 0.12 m range is due to density changes over the upper 100 m of the water column, as determined form climatological temperature and salinity data. A similar range is found in analyses of satellite altimetry. These deep ocean influences are observed in the coastal sea level observations, where in addition are the inner shelf effects due to the locally driven seasonal cycle of the circulation.

Thus the seasonal cycle in atmospheric pressure adjusted coastal sea level partitions roughly 1/3 (0.06 m), 2/3rds (0.12 m) between local dynamic and deep ocean static effects. The inverted barometer effect by atmospheric pressure adds about another 0.06 m to the climatological range in annual sea level. Granted, this may be a simplified viewpoint for several reasons. Shallow water wintertime temperatures are cooler than deeper offshore waters and conversely in summertime, imparting baroclinic effects. Similarly, fresh water buoyancy inputs from local land drainage and from remote rivers to the north complicate the baroclinic structure across the entire shelf seasonally. In addition, with the internal Rossby radius of deformation, $R_0 = NH/f$, varying with stratification, just how far inward from the shelf break deep ocean dynamical influences extend is itself variable. It is perhaps for these reasons that only over the inner shelf, where the dynamical effects of local wind and buoyancy effects are themselves well defined, do we find a statistically robust seasonal cycle. Notwithstanding the need for continued analyses of episodic events, the above apportionment between local dynamical and offshore static influences on the seasonal variations in central WFS currents and sea level appears to provide a physically reasonable baseline for the observations. The seasonal dynamical anomalies to the circulation add to the long term mean circulation (e.g. Weisberg et al., 2009b), which is directed down coast.

Such well-organized, fully three-dimensional WFS coastal ocean circulation patterns identified on long-term average (Weisberg et al., 2009b), at synoptic scales (e.g., Weisberg et al., 2005, 2009a) and now at seasonal scales have important implications for fisheries, harmful algae and other ecological phenomena (e.g., Steidinger, 1975; Tester and Steidinger ,1997; Werner et al., 1997; Walsh et al., 2006, 2011; Weisberg, 2011). Revealed by an unprecedented set of WFS observations, and explained on the basis of local forcing and deep ocean influences, these findings amplify the need for sustaining coastal ocean circulation observations within the context of scientifically defensible, multidisciplinary, coordinated coastal ocean observing and modeling systems. Only over limited coastal ocean regions with sustained observations have we been able to identify monthly mean climatologies for circulation with quantifying error bars (e.g., Blanton et al., 2003; Winant et al., 2003; Lentz, 2008; Brink et al., 2009). Moreover, as useful as climatologies may be in providing overviews, the intraseasonal to interannual events occurring about these climatologies may be even of more importance in understanding and predicting ecosystems behaviors. Given that the coastal ocean is where society meets the sea, the need for sustained, systematic, multidisciplinary ocean observations in coordination with models requires attention.

Acknowledgments

The primary data used herein derive from observations that began in 1993 under an initial USGS cooperative agreement with USF and were sustained largely since 1998 by programs or grants from the State of Florida, ONR, MMS, NOAA and NSF. Present support is by ONR Grant # N00014-10-1-0785, NOAA Grant #s NA06NOS4780246 and NA07NOS4730409, the first being for the ECOHAB program and the second being for the SECOORA program, and NSF Grant # OCE-0741705. The CMS-USF Ocean Circulation Group staff are responsible for the success of the field program (J. Law, C. Merz and (formerly) R. Cole) as assisted with data management and processing support (J. Donovan, P. Smith and D.A. Mayer). D. Mayer also provided many useful discussions on the climatological averages. This is CPR contribution #24.

References

Alvera-Azcárate, A., Barth, A., Beckers, J.-M., Weisberg, R.H., 2007. Multivariate reconstruction of missing data in sea surface temperature, chlorophyll, and wind satellite fields. Journal of Geophysical Research 112, C03008. http://dx.doi.org/10.1029/2006JC003660.

Alvera-Azcárate, A., Barth, A., Weisberg, R.H., 2009. The surface circulation of the Caribbean Sea and the Gulf of Mexico as inferred from satellite altimetry. Journal of Physical Oceanography 39, 640–657.

Antonov, J.I., Locarnini, R.A., Boyer, T.P., Mishonov, A.V., Garcia, H.E., 2006. World Ocean Atlas 2005, Salinity. In: Levitus, S. (Ed.), NOAA Atlas NESDIS 62, vol. 2. US Government Printing Office, Washington, DC, p. 182.

Beron-Vera, F.J., Olascoaga, M.J., 2009. An assessment of the importance of chaotic stirring and turbulent mixing on the West Florida Shelf. Journal of Physical Oceanography 39, 1743–1755.

Blaha, J., Sturges, W., 1981. Evidence for wind-forced circulation in the Gulf of Mexico. Journal of Marine Research 39, 771–833.

Blanton, J.O., Amft, J.A., Lee, D.K., Riordan, A., 1989. Wind stress and heat fluxes observed during winter and spring 1986. Journal of Geophysical Research 94, 10686–10698.

Blanton, B.O., Aretxabaleta, A., Werner, F.E., Seim, H., 2003. Monthly climatology of the continental shelf waters of the South Atlantic Bight. Journal of Geophysical Research 108 (C8), 3264. http://dx.doi.org/10.1029/2002JC001609.

Boicourt, W.C., Wiseman Jr., W.J., Valle-Levinson, A., Atkinson, L.P., 1998. Continental shelf of the southeastern United States and the Gulf of Mexico: in the shadow of the western boundary current. In: Robinson, A.R., Brink, K.H. (Eds.), The Sea. John Wiley & Sons Inc., New York, pp. 135–181.

Brink, K.H., Beardsley, R.C., Limeburner, R., Irish, J.D., Caruso, M., 2009. Long-term moored array measurements of currents and hydrography over Georges Bank: 1994–1999. Progress in Oceanography 82 (3), 191–223. http://dx.doi.org/10.1016/j.pocean.2009.07.004.

Carlson, D.F., Clarke, A.J., 2009. Seasonal along-isobath geostrophic flows on the west Florida shelf with application to Karenia brevis red tide blooms in Florida's Big Bend. Continental Shelf Research 29, 445–455.

Carnes, M.R., Teague, W.J., Jarosz, E., 2008. Low-frequency current variability observed at the shelfbreak in the northeastern Gulf of Mexico: November 2004–May 2005. Continental Shelf Research 28 (3), 399–423. http://dx.doi.org/10.1016/j.csr.2007.10.005.

Chao, Y., Li, Z., Farrara, J.D., Huang, P., 2009. Blended sea surface temperatures from multiple satellites and in-situ observations for coastal oceans. Journal of Atmospheric and Oceanic Technology 26, 1415–1426.

Cragg, J., Mitchum, G., Sturges, W., 1983. Wind-induced sea-surface slopes on the West Florida Shelf. Journal of Physical Oceanography 13, 2201–2212.

DiMarco, S.F., Nowlin, W.D., Reid, R.O., 2005. A statistic description of the velocity fields from upper ocean drifters in the Gulf of Mexico. In: Sturges, W., Lugo-Fernandez, A., (Eds.), Circulation in the Gulf of Mexico: Observations and Models, Geophysical Monograph 161, American Geophysical Union, pp 101–110.

Ducet, N., Le Traon, P.-Y., Reverdin, G., 2000. Global high resolution mapping of ocean circulation from Topex/Poseidon and ERS-1 and -2. Journal of Geophysical Research 105 (C8), 19477–19498.

Dzwonkowski, B., Park, K., 2010. Influence of wind stress and discharge on the mean and seasonal currents on the Alabama shelf of the northeastern Gulf of Mexico. Journal of Geophysical Research 115, C12052. http://dx.doi.org/10.1029/2010JC006449.

Emery, W.J., Thomson, R.E., 2001. Data Analysis Methods in Physical Oceanography (2nd edition). Elsevier Science, Amsterdam, 638 pp.

Fewings, M., Lentz, S.J., Fredericks, J., 2008. Observations of cross-shelf flow driven by cross-shelf winds on the inner continental shelf. Journal of Physical Oceanography 38, 2358–2378.

Hallock, Z.R., Teague, W.J., Jarosz, E., 2009. Subinertial slope-trapped waves in the northeastern Gulf of Mexico. Journal of Physical Oceanography 39, 1475–1485.

Halper, F.B., Schroeder, W.W., 1990. The response of shelf waters to the passage of tropical cyclones – observations from the Gulf of Mexico. Continental Shelf Research 10, 777–793.
He, R., Weisberg, R.H., 2002. Tides on the west Florida Shelf. Journal of Physical Oceanography 32, 3455–3473.
He, R., Weisberg, R.H., 2003. A Loop Current intrusion case study on the West Florida Shelf. Journal of Physical Oceanography 33, 465–477.
He, R., Liu, Y., Weisberg, R.H., 2004. Coastal ocean wind fields gauged against the performance of an ocean circulation model. Geophysical Research Letters 31, L14303. http://dx.doi.org/10.1029/2003GL019261.
Huh, O., Wiseman, W.J., Rouse, L., 1981. Intrusion of loop current onto the west Florida continental shelf. Journal of Geophysical Research 86, 4186–4192.
Kara, A.B., Wallcraft, A.J., Hurlburt, H.E., 2007. A correction for land contamination of atmospheric variables near land–sea boundaries. Journal of Physical Oceanography 37, 803–818.
Kara, A.B., Wallcraft, A.J., Barron, C.N., Hurlburt, H.E., Bourassa, M.A., 2008. Accuracy of 10 m winds from satellites and NWP products near land-sea boundaries. Journal of Geophysical Research 113, C10020. http://dx.doi.org/10.1029/2007JC004516.
Kistler, R.E., Coauthors, 2001. The NCEP-NCAR 50-year reanalysis: monthly means CD-ROM and documentation. Bulletin of American Meteorological Society 82 (2), 247–268.
Large, W.G., Pond, S., 1981. Open ocean momentum flux measurements in moderate to strong winds. Journal of Physical Oceanography 11, 324–336.
Le Traon, P.Y., Faugère, Y., Hernandez, F., Dorandeu, J., Mertz, F., Ablain, M., 2003. Can we merge GEOSAT follow-on with TOPEX/POSEIDON and *ERS*-2 for an improved description of the ocean circulation? Journal of Atmospheric and Oceanic Technology 20, 889–895.
Lentz, S.J., 2008. Seasonal variations in the circulation over the Middle Atlantic Bight continental shelf. Journal of Physical Oceanography 38, 1486–1500.
Li, Z., Weisberg, R.H., 1999a. West Florida Shelf response to upwelling favorable wind forcing: kinematics. Journal of Geophysical Research 104, 13507–13527.
Li, Z., Weisberg, R.H., 1999b. West Florida continental shelf response to upwelling favorable wind forcing, Part II: Dynamical analyses. Journal of Geophysical Research 104, 23427–23442.
Liu, Y., Weisberg, R.H., 2005a. Momentum balance diagnoses for the West Florida Shelf. Continental Shelf Research 25, 2054–2074. http://dx.doi.org/10.1016/j.csr.2005.03.004.
Liu, Y., Weisberg, R.H., 2005b. Patterns of ocean current variability on the West Florida Shelf using the self-organizing map. Journal of Geophysical Research 110, C06003. http://dx.doi.org/10.1029/2004JC002786.
Liu, Y., Weisberg, R.H., 2007. Ocean currents and sea surface heights estimated across the West Florida Shelf. Journal of Physical Oceanography 37 (6), 1697–1713. http://dx.doi.org/10.1175/JPO3083.1.
Liu, Y., Weisberg, R.H., 2011. Evaluation of trajectory modeling in different dynamic regions using normalized cumulative Lagrangian separation. Journal of Geophysical Research 116, C09013. http://dx.doi.org/10.1029/2010JC006837.
Liu, Y., Liang, X.S., Weisberg, R.H., 2007. Rectification of the bias in the wavelet power spectrum. Journal of Atmospheric and Oceanic Technology 24, 2093–2102. http://dx.doi.org/10.1175/2007JTECHO511.1.
Liu, Y., MacFadyen, A., Ji, Z.-G., Weisberg, R.H. (Eds.), 2011a. Monitoring and Modeling the Deepwater Horizon Oil Spill: A Record-Breaking Enterprise. Geophysical Monograph Series 195. AGU/Geopress, Washington, DC. ISSN 0065–8448, ISBN 978-0-87590-485-6, p. 271, http://dx.doi.org/10.1029/GM195.
Liu, Y., Weisberg, R.H., Hu, C., Kovach, C., Riethmüller, R., 2011b. Evolution of the Loop Current system during the Deepwater Horizon oil spill event as observed with drifters and satellites. In: Monitoring and Modeling the Deepwater Horizon Oil Spill: A Record-Breaking Enterprise, Geophysical Monograph Series, vol. 195, pp. 91–101. http://dx.doi.org/10.1029/2011GM001127.
Locarnini, R.A., Mishonov, A.V., Antonov, J.I., Boyer, T.P., Garcia, H.E., 2006. World Ocean Atlas 2005, Temperature. In: Levitus, S. (Ed.), NOAA Atlas NESDIS 61, vol. 1. US Government Printing Office, Washington, DC, p. 182.
Marmorino, G.O., 1982. Wind-forced sea level variability along the West Florida Shelf. Journal of Physical Oceanography 12, 389–404.
Marmorino, G.O., 1983a. Small-scale variations of the wind-driven coastal sea level response in the West Florida Bight. Journal of Physical Oceanography 13, 93–102.
Marmorino, G.O., 1983b. Variability of current, temperature, and bottom pressure across the West Florida continental shelf, winter, 1981–1982. Journal of Geophysical Research 88 (C7), 4439–4457.
Mayer, D.A., Virmani, J.I., Weisberg, R.H., 2007. Velocity comparisons from upward and downward acoustic Doppler current profilers on the West Florida Shelf. Journal of Atmospheric and Oceanic Technology 24, 1950–1960.
Mesinger, F., Coauthors, 2006. North American regional reanalysis. Bulletin of American Meteorological Society 87, 343–360. http://dx.doi.org/10.1175/BAMS-B7-3-343.
Meyers, S.D., Siegel, E.M., Weisberg, R.H., 2001. Observations of currents on the west Florida shelf break. Geophysical Research Letters 28, 2037–2040.
Mitchum, G.T., Clarke, A.J., 1986a. The frictional nearshore response to forcing by synoptic scale winds. Journal of Physical Oceanography 16, 934–946.
Mitchum, G.T., Clarke, A.J., 1986b. Evaluation of frictional, wind-forced long-wave theory on the West Florida Shelf. Journal of Physical Oceanography 16, 1029–1037.
Mitchum, G.T., Sturges, W., 1982. Wind-driven currents on the west Florida shelf. Journal of Physical Oceanography 12, 1310–1317.
Molinari, R.L., Baig, S., Behringer, D.W., Maul, G.A., Legeckis, R., 1977. Winter intrusions of the loop current. Science 198, 505–506.
Niiler, P.P., 1976. Observations of low-frequency currents on the West Florida continental shelf. Memoires Societe Royale des Sciences de Liege 6 X, 331–358.
Ohlmann, J.C., Niiler, P.P., 2005. Circulation over the continental shelf in the northern Gulf of Mexico. Progress in Oceanography 64, 45–81.
Olascoaga, M.J., Beron-Vera, F.J., Brand, L.E., Kocxak, H., 2008. Tracing the early development of harmful algal blooms with the aid of Lagrangian coherent structures. Journal of Geophysical Research 113, C12014. http://dx.doi.org/10.1029/2007JC004533.
Paluszkiewicz, K., Atkinson, L.P., Posmentier, E.S., McClain, C.R., 1983. Observations of a loop current frontal eddy intrusion onto the west Florida shelf. Journal of Geophysical Research 88, 9639–9651.
Pascual, A., Faugère, F., Larnicol, G., Le Traon, P.Y., 2006. Improved description of the ocean mesoscale variability by combining four satellite altimeters. Geophysical Research Letters 33, L02611.
Pawlowicz, R., Beardsley, B., Lentz, S., 2002. Classical tidal harmonic analysis including error estimates in MATLAB using T-TIDE. Computers & Geosciences 28, 929–937.
Perlin, N., Samelson, R.M., Chelton, D.B., 2004. Scatterometer and model wind and wind stress in the Oregon–northern California coastal zone. Monthly Weather Review 132, 2110–2129.
Price, J.F., Mooers, C.N.K., VanLeer, J.C., 1978. Observation and simulation of storm-induced mixed-layer deepening. Journal of Physical Oceanography 8, 582–599.
Price, J.M., Reed, M., Howard, M.K., Johnson, W.R., Jia, Z.G., Marshall, C.F., Guinasso, N.J.J., Rainey, G.B., 2006. Preliminary assessment of an oil-spill trajectory model using satellite-tracked, oil-spill-simulating drifters. Environmental Modelling and Software 21, 258–270.
Risien, C.M., Chelton, D.B., 2008. A global climatology of surface wind and wind stress fields from eight years of QuikSCAT Scatterometer data. Journal of Physical Oceanography 38, 2379–2413.
Smith, S.R., Jacobs, G.A., 2005. Seasonal circulation fields in the northern Gulf of Mexico calculated by assimilating current meter, shipboard ADCP, and drifter data simultaneously with the shallow water equations. Continental Shelf Research 25, 157–183. http://dx.doi.org/10.1016/j.csr.2004.09.010.
Steidinger, K.A., 1975. Implications of dinoflagellate life cycles on initiation of *Gymnodinium breve* red tides. Environmental Letters 9, 129–139.
Sturges, W., Leben, R., 2000. Frequency of ring separations from the Loop Current in the Gulf of Mexico: a revised estimate. Journal of Physical Oceanography 30, 1814–1819.
Tester, P.A., Steidinger, K.A., 1997. *Gymnodinium breve* red tide blooms: initiation, transport and consequences of surface circulation. Limnology and Oceanography 42, 1039–1051.
Tilburg, C.E., 2003. Across-shelf transport on a continental shelf: do across-shelf winds matter? Journal of Physical Oceanography 33, 2675–2688.
Tolbert, W.H., Salsman, G.G., 1964. Surface circulation of the eastern Gulf of Mexico as determined by drift-bottled studies. Journal of Geophysical Research 69, 223–230.
Torrence, C., Compo, G.P., 1998. A practical guide to wavelet analysis. Bulletin of American Meteorological Society 79, 61–78.
Virmani, J.I., Weisberg, R.H., 2003. Features of the observed annual ocean-atmosphere flux variability on the West Florida Shelf. Journal of Climate 16, 734–745.
Vukovich, F.M., 2007. Climatology of ocean features in the Gulf of Mexico using satellite remote sensing data. Journal of Physical Oceanography 37, 689–707.
Walsh, J.J. et al., 2006. Red tides in the Gulf of Mexico: where, when, and why? Journal of Geophysical Research 111, C11003. http://dx.doi.org/10.1029/2004JC002813.
Walsh, J.J., Tomas, C.R., Steidinger, K.A., Lenes, J.M., Chen, F.R., Weisberg, R.H., Zheng, L., Landsberg, J.H., Vargo, G.A., Heil, C.A., 2011. Imprudent fishing harvests and consequent trophic cascades on the West Florida Shelf over the last half century: a harbinger of increased human deaths from paralytic shellfish poisoning along the southeastern United States in response to oligotrophication. Continental Shelf Research 31, 891–911. http://dx.doi.org/10.1016/j.csr.2011.02.007.
Weatherly, G.L., Martin, P.J., 1978. On the structure and dynamics of the oceanic bottom boundary layer. Journal of Physical Oceanography 8, 557–570.
Weatherly, G.L., Thistle, D., 1997. On the wintertime currents in the Florida Big Bend region. Continental Shelf Research 17, 1297–1319.
Weisberg, R.H., 2011. Coastal ocean pollution, water quality and ecology: a commentary. MTS Journal 45 (2), 35–42.
Weisberg, R.H., He, R., 2003. Local and deep-ocean forcing contributions to anomalous water properties on the West Florida Shelf. Journal of Geophysical Research 108 (C6), 3184. http://dx.doi.org/10.1029/2002JC001407.
Weisberg, R.H., Black, B.D., Yang, H., 1996. Seasonal modulation of the west Florida continental shelf circulation. Geophysical Research Letters 23, 2247–2250.
Weisberg, R.H., Black, B.D., Li, Z., 2000. An upwelling case study on Florida's west coast. Journal of Geophysical Research 105, 11459–11469.
Weisberg, R.H., Li, Z., Muller-Karger, F.E., 2001. West Florida shelf response to local wind forcing: April 1998. Journal of Geophysical Research 106, 31239–31262.
Weisberg, R.H., He, R., Liu, Y., Virmani, J., 2005. West Florida shelf circulation on synoptic, seasonal, and inter-annual time scales. In: Sturges, W., Lugo-Fernandez, A. (Eds.), Circulation in the Gulf of Mexico: Observations and Models, Geophysical Monograph 161. American Geophysical Union, pp. 325–347.

Weisberg, R.H., Barth, A., Alvera-Azcárate, A., Zheng, L., 2009a. A coordinatedcoastal ocean observing and modeling system for the West Florida Shelf. Harmful Algae 8, 585–598.

Weisberg, R.H., Liu, Y., Mayer, D.A., 2009b. West Florida Shelf mean circulation observed with long-term moorings. Geophysical Research Letters 36, L19610. http://dx.doi.org/10.1029/2009GL040028.

Werner, F.E., Quinlan, J.A., Blanton, B.O., Luettich Jr., R.A., 1997. The role of hydrodynamics in explaining variability in fish populations. Journal of Sea Research 37, 195–212.

Winant, C.D., Dever, E.P., Hendershott, M.C., 2003. Characteristic patterns of shelf circulation at the boundary between central and southern California. Journal of Geophysical Research 108 (C2), 3021. http://dx.doi.org/10.1029/2001JC001302.

Yang, H., Weisberg, R.H., 1999. West Florida continental shelf circulation response to climatological wind forcing. Journal of Geophysical Research 104, 5301–5320.

Yang, H., Weisberg, R.H., Niiler, P.P., Sturges, W., Johnson, W., 1999. Lagrangian circulation and forbidden zone on the West Florida Shelf. Continental Shelf Research 19, 1221–1245.